MICROCOPY RESOLUTION TEST CHART
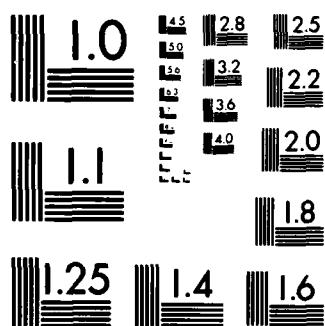
NATIONAL BUREAU OF STANDARDS-1963-A

AFGL-TR-83-0031
PHYSICAL SCIENCES RESEARCH PAPERS, NO. 665

# O-Atom Yields From Microwave Discharges in $N_2O$/Ar Mixtures

L. G. PIPER
W. T. RAWLINS
R. A. ARMSTRONG

DTIC
SELECTED
JUL 20 1983
S          D
B

1 February 1983

OPTICAL PHYSICS DIVISION                    PROJECT 2310

**AIR FORCE GEOPHYSICS LABORATORY**

HANSCOM AFB, MASSACHUSETTS 01731

## AIR FORCE SYSTEMS COMMAND, USAF

This report has been reviewed by the ESD Public Affairs Office (PA) and is releasable to the National Technical Information Service (NTIS).

This technical report has been reviewed and is approved for publication.

DR. ALVA T. STAIR, Jr
Chief Scientist

A130 429

## O-ATOM YIELDS FROM MICROWAVE DISCHARGES IN N₂O/Ar MIXTURES

Scientific. Interim.

PSRP No. 665

T.G. Piper
J.J. Raskin
R.A. Armstrong

Air Force Geophysics Laboratory (OPR-1)
Hanscom AFB
Massachusetts 01731

61102F
2310G414

Air Force Geophysics Laboratory (OPR-1)
Hanscom AFB
Massachusetts 01731

1 February 1983

50

Unclassified

Physical Science, Inc.
Research Park
Andover, Mass. 01810

O-atoms                    N-atoms
Microwave discharge        Kinetics
N₂O

We have studied the products of Ar/$N_2O$ microwave discharges to determine their fitness as sources of atomic oxygen in discharge-flow reactors. For $N_2O$ feed rates below 10-20 $\mu$mol s$^{-1}$, the discharge converts about 75 percent of the $N_2O$ to atomic oxygen, and in addition, produces small quantities of atomic nitrogen, generally less than 10 percent of the O-atom product. At higher $N_2O$ feed rates the O-atom production efficiency decreases, and some nitric oxide accompanies the O-atoms out of the discharge

DD 1473

20. Abstract (Contd)

At some intermediate $N_2O$ feed rate, the exact point being a function of the discharge power and the $Ar/N_2O$ mixing ratio, neither N nor NO leaves the discharge, only atomic oxygen. Adding molecular nitrogen to the discharge also eliminates any NO product, but at the penalty of a slightly reduced O-atom production efficiency. We have produced atomic oxygen flows in excess of $20\ \mu mol\ s^{-1}$ at pressures near 1 Torr and discharge powers of only 30 W.

We have developed a kinetic model of the discharge to help explain the experimental observations. Our model reproduces our experimental observations reasonably well only if the electron-impact dissociation of the $N_2O$ in the discharge proceeds through a spin-forbidden channel to produce $O(^3P)$, and if, in addition, about 20 percent of the $N_2O$ dissociations result from collisions between metastable Ar atoms in the discharge and $N_2O$.

# Contents

| Accession For | |
|---|---|
| NTIS GRA&I | ✔ |
| DTIC TAB | ☐ |
| Unannounced | ☐ |
| Justification | |
| By | |
| Distribution/ | |
| Availability Codes | |
| Dist | Avail and/or Special |
| *A* | |

## Illustrations

# O-Atom Yields From
# Microwave Discharges in N₂O/Ar Mixtures

## 1. INTRODUCTION

Atomic oxygen *sources* for flow reactors take a variety of forms, and each
has its own particular strengths and weaknesses. The simplest technique for
making atomic oxygen is to dissociate molecular oxygen, usually in some form
of discharge, the 2.45-GHz microwave discharges being most common.[1] These
sources are somewhat limited in overall yield and generally produce large
quantities of accompanying electronically-excited metastable singlet molecular
oxygen $- O_2 (a\ ^1\Delta_g,\ b\ ^1\Sigma_g^+).$ [2-5] In pure molecular oxygen the dissociation
efficiency is generally only a few percent.[5] If the oxygen is highly diluted in a

1. Howard, C.J. (1979) Kinetic measurements using flow tubes, J. Phys. Chem.
   83:3.

2. Elias, L., Ogryzlo, E.A., and Schiff, H.I. (1959) The study of electrically
   discharged O₂ by means of an isothermal calorimetric detector,
   Can. J. Chem. 37:1680.

3. Mathias, A., and Schiff, H.I. (1964) Discussions Faraday Soc. 37:38.

4. March, R.E., Furnival, S.G., and Schiff, H.I. (1965) Photochem. Photobiol.
   4:971.

5. Cook, T.J., and Miller, T.A. (1974) Production of $^1\Delta_g$ O₂ from microwave
   discharges in CO₂, NO₂ and SO₂, Chem. Phys. Lett. 25:396.

rare gas buffer such as Ar or He, dissociation efficiencies can exceed 50 per-
cent,[5,6] but due to the large dilution, the overall atomic oxygen yield is still low.

The other major technique is to convert N-atoms to O-atoms by titration with
NO:

$$N + NO \rightarrow N_2 + O \quad . \tag{1}$$

This technique has the advantage that the absolute flow rates will be equal to the
flow rate of the nitric oxide added, provided atomic nitrogen is in excess and that
the measurements requiring the oxygen atoms are made before they have a chance
to recombine. If significant recombination obtains, a large fraction of the molec-
ular oxygen formed in the atomic recombination will be $O_2(a\ ^1\Delta_g)$.[8] The yields
of atomic nitrogen from conventional discharge sources are generally even lower
than those from oxygen discharges, so the maximum O-atom flow rates again are
limited.

The thermal decomposition of $O_2$, $O_3$, or $N_2O$ in contact with a Nernst glower
is also useful for certain applications.[9,10] The claims for the lack of reactive-
impurity production by this technique are mixed, and yields are small, being
limited to atomic-oxygen flow rates less than a micromole $s^{-1}$.[9]

Photolysis of molecular oxygen or some other oxygen-donating species with
vacuum ultraviolet laser pulses provides a potentially very clean source of atomic
oxygen.[11] Producing radially and axially uniform number densities of O-atoms
in the flow tube, however, requires extreme care. In addition, current laser
development limits this technique to atomic-oxygen flow rates on the order of
$.1\ \mu mol\ s^{-1}$ or less.

Several years ago, Ung claimed that microwave discharges through mixtures
of $Ar/N_2O/N_2$ would produce copious quantities of atomic oxygen, free from
molecular oxygen.[12] He deduced atomic-oxygen production rates an order of

6.  Piper, L.G. (1978) Unpublished results.

7.  Kaufman, F., and Kelso, J.R. (1958) Reactions of Atomic Oxygen and Atomic
    Nitrogen With Oxides of Nitrogen, 7th Int. Symp. Combustion, p. 53.

8.  Black, G., and Slanger, T.G. (1981) Production of $O_2(a\ ^1\Delta_g)$ by oxygen atom
    recombination on a Pyrex $^D$ surface, J. Chem. Phys. 74:617.

9.  Lunden, O.R., Ketcheson, R.D., and Schiff, H.I. (1969) The Production of
    $O(^3P)$ Atoms, Free From Excited Molecules, and Their Reaction With $O_2$,
    12th Int. Symp. Combustion, p. 307.

10.  McCrumb, J.L., and Kaufman, F. (1972) Kinetics of the $O + O_3$ reaction,
    J. Chem. Phys. 57:1270.

11.  Rawlins, W.T., Piper, L.G., Caledonia, G.E., and Green, B.D. (1981)
    COCHISE Research, Physical Sciences Inc., TR-298.

12.  Ung, A.Y.M. (1975) A microwave discharge in $N_2O$-$N_2$ mixtures: A prolific
    source of oxygen atoms, Chem. Phys. Lett. 32:351.

magnitude greater with $N_2O$ discharges than he could obtain using a molecular-oxygen discharge operating under the same conditions. His measured yields were not particularly impressive, a maximum O-atom flow rate of 0.5 $\mu$mol s$^{-1}$, but the atomic oxygen his discharge produced clearly suffered severe depletion by recombination between his discharge and detector.

Intrigued by Ung's results, and needing to find a technique to produce relative-ly large flows of atomic-oxygen without large accompanying flows of molecular oxygen, we began to investigate further the characteristics of $Ar/N_2O$ discharges. Using a discharge-flow apparatus to measure the air-afterglow intensity[16,17] as a function the number density of nitric oxide injected downstream of the discharge, we determined number densities of atomic-oxygen and either atomic-nitrogen or nitric-oxide products in the discharged gases. While our results will not support Ung's claim that oxygen-atom production is an order of magnitude more efficient using $N_2O$ as the discharge gas as opposed to molecular oxygen, they do show that $Ar/N_2O$ discharges produce large flow rates of atomic oxygen and that furthermore, under certain conditions negligible flow rates of atomic nitrogen or nitric oxide accompany the atomic-oxygen flow.

## 2. EXPERIMENTAL

### 2.1 Apparatus

The apparatus is a modification of one we have used previously in a number of other studies.[15-19] It consists of a 2-in. flow tube pumped by a Leybold-Heraeus Roots blower/forepump combination capable of producing linear velocities

13. Kaufman, F. (1958) The air afterglow and its use in the study of some reactions of atomic oxygen, Proc. Roy. Soc. (London) 247A:123.

14. Kaufman, F. (1973) The air afterglow revisited in Chemiluminescence and Bioluminescence, M. J. Cormier, D. M. Hercules, and J. Lee, Eds., pp. 83-100.

15. Piper, L.G., Caledonia, G.E., and Kennealy, J.P. (1981a) Rate constants for deactivation of $N_2(A)v'=0, 1$ by $O_2$, J. Chem. Phys. 74:2888.

16. Piper, L.G., Caledonia, G.E., and Kennealy, J.P. (1981b) Rate constants for deactivation of $N_2(A\ ^3\Sigma_u^+, v'=0, 1)$ by O, J. Chem. Phys. 75:2847.

17. Piper, L.G. (1982) The excitation of $O(^1S)$ in the reaction between $N_2(A\ ^3\Sigma_u^+)$ and $O(^3P)$, J. Chem. Phys. 77:2373.

18. Rawlins, W.T., and Piper, L.G. (1981) Effects of excitation mechanism on linewidth parameters of conventional vacuum ultraviolet (VUV) discharge line sources, Proc. Soc. Photo.-Opt. Instrum. Eng. 279:58.

19. Piper, L.G., Clyne, M.A.A., and Monkhouse, P.B. (1982) Electronic energy transfer between metastable argon atoms and ground-state oxygen atoms, J. Chem. Soc. Faraday Trans. II 78:1373.

up to $5 \times 10^3$ cm s$^{-1}$ at pressures of 1 torr. The flow-tube apparatus [...]
(see Figure 1), with separate source, reaction, and detection sections that [...]
together with O-ring joints. The detector head is a rectangular stainless-steel
block bored out internally to a 2-in. circular cross section and coated with
Teflon[R] (Dupont Poly-Tef No. [...] 852-201) to retard surface recombination of
atoms.[20] The surface was primed with black primer prior to the Teflon coating
to reduce scattered light inside the block. Two viewing positions consisting of
four circular ports each on the four faces of the block are separated by a distance
of [...] cm. The circular ports, all of which contain MgF$_2$ windows, accommo-
date vacuum ultraviolet resonance lamps, monochromator interface, laser
delivery side-arms, or in the case of these studies, a spatial filter/photo-
multiplier/interference filter combination.

The experiments required two types of optical measurements. A [...]-m
monochromator/thermoelectrically-cooled photomultiplier (EMI 9 [...]A)/photon-
counting rate meter (PARC 1105) combination determined the chemiluminescence
spectra in the flow tube between 185 and 800 nm under a variety of conditions to
support the interpretation of the bulk of the measurements that used a filtered
photomultiplier.
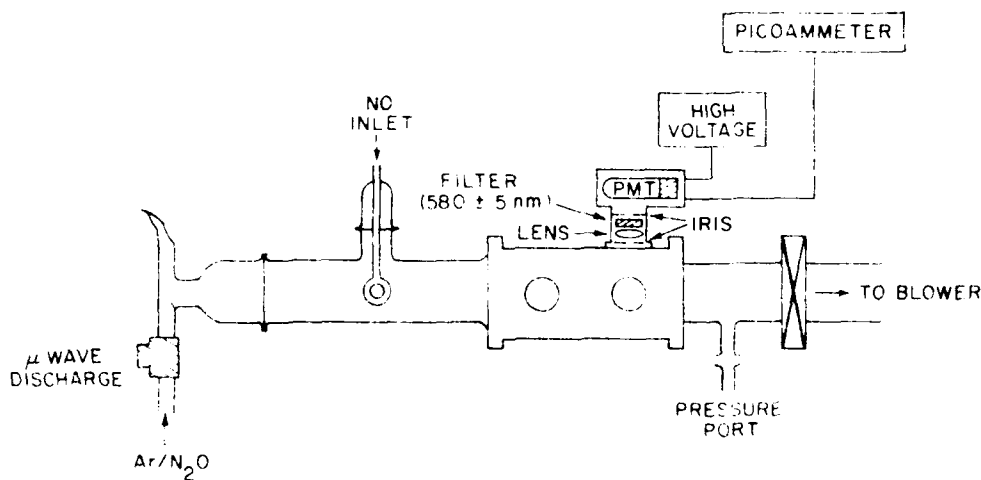


Figure 1.  FAKIR Apparatus Modified for Ar/N$_2$O Discharge Experiments

20.  Berg, H.C., and Kleppner, D. (1962) Rev. Sci. Instr. [...]

... [illegible] ... diameter of the ... [illegible] ... aperture ... [illegible] ... located in front of the lens, 2.3 cm. from the center of the lens hole, while the other aperture was 1-cm. in diameter on plate 14-14 cm. behind the lens. The apertures reduced scattered light from the discharge by a factor of 20.

The interference filter in front of the photomultiplier is centered at 685 nm and has a full-width-at-half-maximum band pass of 10 nm. This wavelength is near the peak of the emission from the $\Delta v = 4$ sequence of the nitrogen first-positive bands when they are excited by atomic-nitrogen recombination, [21] and also is near the peak of the air-afterglow intensity distribution. [22,23] In addition, this band pass is insensitive to chemiluminescence from the nitric oxide/ozone system, which has a short wavelength cutoff of 600 nm, [24] and eliminates the strong argon lines, most of which are to the red of 700 nm, which are scattered from the discharge.

A photomultiplier gain of only $1.5 \times 10^5$ sufficed for all measurements because of the unusually good red response of the photomultiplier (HTV R955). A picoammeter (Keithly 417S)/strip-chart recorder (Heath SR 205) combination chronicled the photomultiplier output.

Flows of argon, nitrous oxide, and, in some cases, nitrogen, pass through a 1-mm o.d. Pyrex (R) tube surrounded by a McCarroll microwave-discharge cavity [25] before entering the main flow tube. Nitric oxide, in a substantial flow ($\approx 7$ per cent of the total flow) of helium joins the discharged gases in the main section of the flow tube through an injector fabricated from a 1-in. diameter loop of 4-mm o.d. polyethylene containing a large number of small holes around both its inner and outer perimeters. The helium flow out of the injector gives injected gases a significant velocity as they enter the main flow, thus aiding their mixing.

Mass-flowmeters determine the flow rates of argon and nitrogen. Rotameter is ... [illegible] of the flow rates ... [illegible] the rate of increase in pressure with time.

21. Golde, M.F., and Thrush, B.A. (1973) Afterglows, Rep. Prog. Phys.
   ... [illegible] ...

22. Fontijn, A., Meyer, C.B., and Schiff, H.I. (1964) Absolute quantum yield measurements of the $NO + O$ reaction and its use as a standard for chemiluminescent reactions, J. Chem. Phys. 4964.

23. Sutoh, M., Morioka, Y., and Nakamura, M. (1980) Absolute rate constant for the ... chemiluminescent combination of atomic oxygen with nitric oxide, J. Chem. Phys. 72, ...

24. Clough, P.N., and Thrash, B.A. (1971) Mechanism of the chemiluminescent reaction between nitric oxide and ozone, Trans. Faraday Soc. ...

25. McCarroll, B. (1970) An improved microwave discharge cavity for 2450 MHz, ... [illegible] ...

in a calibrated volume determines the flow rate of nitric oxide. All flowmeters
were calibrated by measuring rates of increase of pressure with time into ~1.2-
or 1.4-liter flasks, using appropriate differential pressure transducers (Validyne
DP-15), which had themselves been calibrated with silicon oil or mercury
manometers. Typically the flow rates for argon, nitrous oxide, and helium were
1400, 4 to 140, 12 $\mu$mol s$^{-1}$, respectively, the total pressure 1.2 Torr, and
the flow velocity 11 m s$^{-1}$.

The argon and nitrogen flow through molecular-sieve traps to remove $H_2O$
and CO prior to entry into the flow reactor, while the helium flows through the
injector straight from the cylinder. Most experiments used nitrous oxide
(~99.0 percent) straight from the cylinder without further purification. The major
impurity in nitrous oxide is air.[26] We tried removing any air from one lecture
bottle of nitrous oxide by freezing the contents of the bottle with liquid nitrogen
and then pumping on it until the pressure was below 1 mTorr. No volatile residue
remained after a few cycles of thawing, refreezing, and pumping. Experiments
with nitrous oxide purified in this manner gave identical results to those in which
the nitrous oxide was used straight from the cylinder. Nitric oxide, which was
stored in a 5-liter bulb, was purified by flowing slowly at atmospheric pressure and
room temperature through an ascarite trap, then through a trap immersed in a
liquid nitrogen/methanol slush bath (175 K). Final nitric oxide purification
involved several freeze, pump, and thaw cycles of the gas in the storage bulk.
The ascarite trap had been previously baked overnight under vacuum.

## 2.2 Determination of O and N or NO Number Densities by Air-Afterglow Measurements

Mixtures of atomic oxygen and nitric oxide emit a continuum radiation called
the air afterglow, which extends from 375 to beyond 3000 nm.[13,14,22,23,27-31]
The intensity of this emission is directly proportional to the product of the number
densities of atomic oxygen and nitric oxide,[13] and independent of pressure of bath
gas, at least at pressures above about 0.2 Torr.[14] Thus, the emission intensity
of the air afterglow is

$$I_{O/NO} = \kappa(\lambda)[O][NO] \quad , \tag{2}$$

where $\kappa(\lambda)$ is a calibration constant specific to the particular viewing geometry
and incorporates such things as detection system efficiency, the size of the
observation volume, and the absolute air-afterglow rate constant. $\kappa$ is a function

---

Because of the large number of references cited above, they will not be listed
here. See References, page 41.

12

of wavelength both through the detection systems' spectral response as well as through the wavelength variation of the air-afterglow rate constant. Air-afterglow intensity measurements on known number densities of both O and NO determine $\kappa$. Titration of N with NO [Reaction (1)] produces known number densities of atomic oxygen.

In the absence of added nitric oxide, N-atom recombination generates chemiluminescence from the nitrogen first-positive bands, the intensity of which is proportional to the square of the N-atom number density,[21]

$$ N + N \rightarrow N_2 (B^3\Pi_g) $$ (3)

$$ N_2(B) \rightarrow N_2(A^3\Sigma_u^+) + h\nu \quad \text{(first-positive band)} . $$ (4)

Upon addition of NO the first-positive emission intensity decreases until such point as the quantity of NO added balances the amount of N-atoms initially in the flow. At this point, the end point of the NO titration, all N initially in the reactor has quantitatively reacted to form O, and the reactor is dark. Adding even more NO to the reactor produces the air-afterglow emission and the intensity of this emission varies linearly with the amount of NO added.[19] An N-atom titration plot is shown in Fig. 2.

The equation describing the change in the air-afterglow intensity as a function of added [NO] for NO additions beyond the titration end point is

$$ I_{O/NO} = \kappa[O][NO] = \kappa[N]_0([NO]_a - [N]_0) , $$ (5)

where $\kappa$ is the constant of proportionality relating the air-afterglow intensity to the product [O][NO], $[N]_0$ is the number density of N-atoms initially in the reactor prior to NO addition and the O-atom number density for NO additions beyond the titration end point, and $[NO]_a$ refers to the NO number density that would obtain in the absence of Reaction (1). The factor $\kappa$ then is determined to be the ratio of the square of the slope to the intercept of the line describing the change in air-afterglow intensity with $[NO]_a$.

## 2.3 Experimental Technique

The experimental measurements involved monitoring the air-afterglow intensity at three to five different number densities of added nitric oxide. The atomic-oxygen number density is the ratio of the slope of the $I_{O/NO}$ vs $[NO]_{added}$ plot divided by the calibration constant, $\kappa$. An intercept of the $I_{O/NO}$ vs $[NO]$ line on the ordinate indicates that nitric oxide is an $N_2O$-discharge product along with the
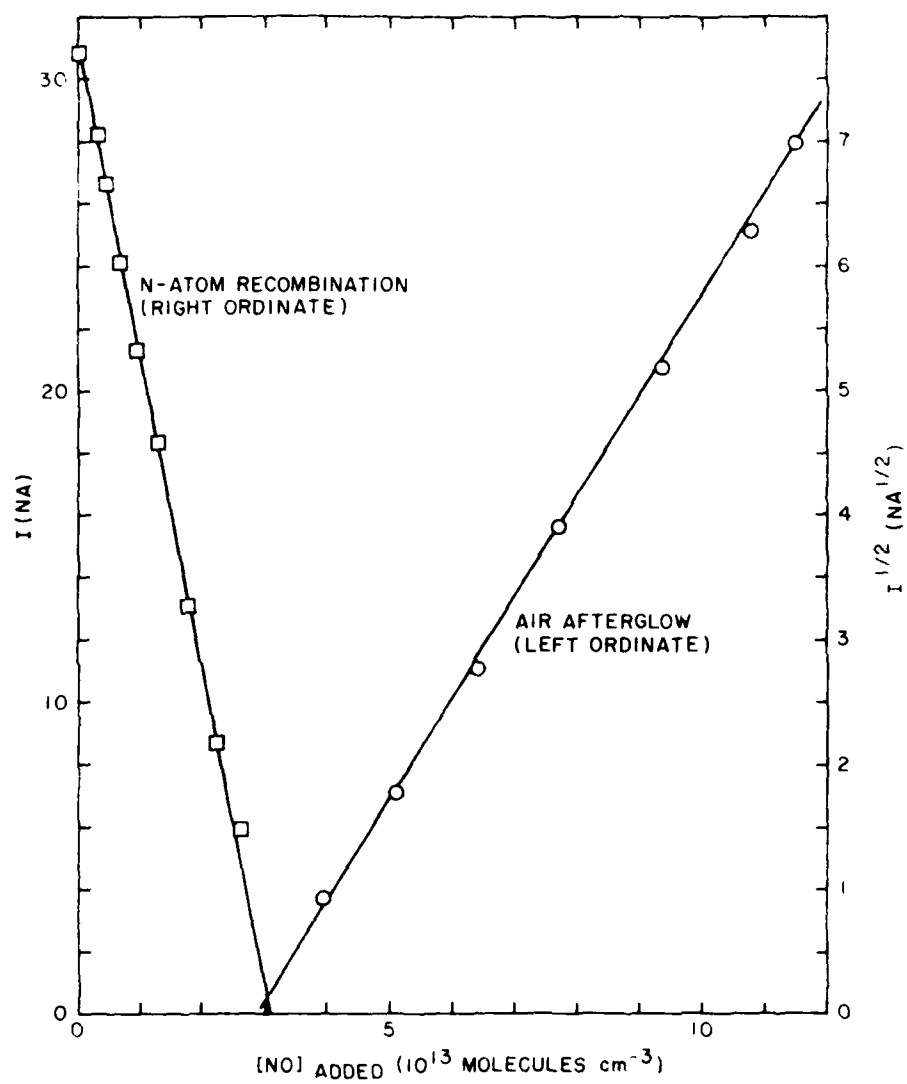
Figure 2. Intensity at 580 nm as a Function of Added NO Number Density for Discharged $Ar/N_2$

atomic oxygen, and the number density of this product NO is the ratio of the intercept to slope of the $I_{O/NO}$ vs [NO] line. An intercept on the abscissa indicates that nitrogen atoms, produced in the $N_2O$ discharge along with the atomic oxygen, consumed some of the added NO. The initial N-atom number density is equal to the added NO number density at the point of intersection of the $I_{O/NO}$ vs [NO] line and the abscissa. O-atom number densities determined from the slope of such plots must be corrected for the additional atomic oxygen made in the titration of the initial N atoms with the NO. The large rate coefficient for Reaction (1)[32-34] and the long flow time from the discharge to the observation point ($\approx$ 45 ms) precludes the possibility that both atomic nitrogen and nitric oxide will coexist as far as the detector.

A series of calibrations taken over a period of time established $\kappa$ to be ±8 percent. The slopes of the $I_{O/NO}$ vs [NO] plots for the determination of [O] had standard deviations less than 5 percent. Thus, the determination of [O] is in principle accurate to ±10 percent.

After determining the O-atom and N-atom or NO number densities, we converted them to flow rates so that we could make reasonable comparisons from one set of conditions to another. This approach affords greater recognition of the similarities and differences between experimental runs. For example, runs with 1400 $\mu$mol s$^{-1}$ of argon through the discharge, generated approximately the same O- and NO-product flow rates from a given input of $N_2O$ whether the pressure was 0.52 or 1.25 Torr. The number densities of the products from the two experiments, however, differed by a factor of 2.5. Under our baseline set of conditions, $F_{Ar} \approx$ 1400 $\mu$mol s$^{-1}$, $F_{He} \approx$ 115 $\mu$mol s$^{-1}$, p $\approx$ 1.2 Torr, and 30 W forward power from the discharge, an atomic-oxygen flow rate of 20 $\mu$mol s$^{-1}$ corresponds to an O-atom number density of about $5 \times 10^{11}$ atoms cm$^{-3}$. In one experiment we produced more than 1/3 Torr of atomic oxygen 150-ms downstream from the discharge at a power of only 30 W.

One complication in using the air-afterglow technique to measure O-atom number densities is the slow removal of atomic oxygen in a three-body recombination reaction with NO:

32. Husain, D., and Slater, N.K.H. (1980) Kinetic study of ground state atomic nitrogen, N(2 $^4S_{3/2}$) by time-resolved atomic resonance fluorescence, J. Chem. Soc. Faraday Trans. II 76:606.

33. Lee, J.H., Michael, J.V., Payne, W.A., and Stief, L.J. (1978) Absolute rate of the reaction of N($^4$S) with NO from 196-400 K with DF-RF and FP-RF techniques, J. Chem. Phys. 69:3069.

34. Clyne, M.A.A., and McDermid, I.S. (1975) Mass spectrometric determinations of the rates of elementary reactions of NO and NO$_2$ with ground state N $^4$S atoms, J. Chem. Soc. Faraday Trans. I 71:2189.

$$O + NO + M \rightarrow NO_2 + M \quad (k_6 = 7 \cdot 10^{-52} \text{ cm}^6 \text{ molecule}^{-2} \text{ s}^{-1} \text{ for } M = Ar)^{35}$$

$$(6)$$

$$O + NO_2 \rightarrow NO + O_2 \quad (k_7 = 9.5 \times 10^{-12} \text{ cm}^3 \text{ molecule}^{-1} \text{ s}^{-1})^{35} \quad . \qquad (7)$$
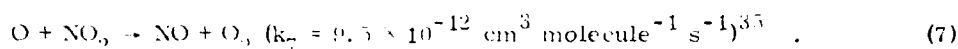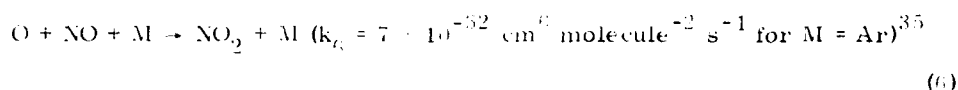
The second reaction is fast, and maintains a constant NO number density, while doubling the effective rate at which O is removed in Reaction (6). The effect of these reactions is strongest at higher pressures ($\geq 1.5$ Torr), longer mixing times ($\geq 30$ ms) and large NO number densities ($\geq 10^{14}$ molecules cm$^{-3}$). Corrections for this effect were generally less than 5 percent in the calibration experiments to determine $\kappa$. However, in a few of the experimental runs at higher pressures, slower flow velocities, and large product nitric-oxide number densities, the corrections were large. These cases required an iterative procedure to correct the data.

Because the nitric-oxide number density is constant along the flow tube, the removal of atomic oxygen by Reactions (6) and (7) is a pseudo-first-order process with a rate coefficient double that appropriate to Reaction (6) alone. Thus, O-atom number densities decay exponentially down the tube:

$$\frac{[O]}{[O]_o} = \exp\left\{ -\frac{6.5 \times 10^{16} k_6 P}{\overline{V}} \left( [NO]_1 z_1 + [NO]_2 z_2 \right) \right\} , \qquad (8)$$

where the pressure, $P$, is in Torr, $\overline{V}$ is the bulk flow velocity, and the subscripts 1 and 2 refer to number densities or distances, $z$, between the discharge and injector and between the injector and detector, respectively. The correction procedure first involves computing approximate O-atom and NO product number densities from the raw air-afterglow data. Second, a set of corrected air-afterglow intensities results from multiplying the observed air-afterglow intensities by the ratio $[O]_o/[O]$ [the inverse of Eq. (8), using the approximate NO number densities determined]. Atomic-oxygen and nitric oxide number densities are then iteratively recomputed from the corrected intensities.

35. Baulch, D. L., Drysdale, D. D., Horne, D. G., and Lloyd, A. C. (1973)
    Evaluated Kinetic Data for High Temperature Reaction. II. Homogeneous
    Gas Phase Reactions of the $H_2 - N_2 - O_2$ System, Butterworths, London.

# 3. RESULTS

## 3.1 General Observations

Figure 3 shows how the emission intensity at 580 nm varies with the flow rate of $N_2O$ through the discharge for several different discharge powers. As the $N_2O$ flow rate increases from zero, the emission intensity rises to a peak, then drops to zero (see inset), increases again very sharply, and finally levels off at the highest $N_2O$ flow rates. The color of the chemiluminescence is yellow-orange at low flow rates, changes to a very faint blue near where the 580-nm signal drops to zero, and finally turns grey-green at high $N_2O$ flow rates. While the observed color changes, and the subsequent results of the O, N, and NO number density measurements suggested a fairly obvious interpretation of these observations, we took spectra of the emissions in the reactor under several different sets of conditions so that our interpretation would be unequivocal.

Figure 4 displays the ultraviolet spectrum in our reactor. It is strongest at $N_2O$ flow rates between those giving the initial small 580-nm intensity peak and the dark point. Prominent spectral features of the NO $\gamma$-, $\delta$-, and $\epsilon$-bands show the excitation of the molecule by three-body recombination of O and N atoms.[36,37] For $N_2O$ additions past those giving the 580-nm dark point, this spectrum is completely extinguished.

Figures 5 and 6 show the spectra between 500 and 600 nm when the $N_2O$ flow rates are adjusted to give the initial 580-nm intensity peak and to give the strong grey-green emission occurring after the dark point in the $I_{580}$ vs $F_{N_2O}$ plot, respectively. The spectrum in Figure 5 shows the nitrogen first-positive ($B\ ^3\Pi_g \rightarrow A\ ^3\Sigma_u^+$) band with a vibrational distribution peaked at vibrational levels 10, 11, and 12, characteristic of three-body N-atom recombination.[24] Figure 5 also shows the 558-nm line from OI ($^1S \rightarrow ^1D$) and the $O_2(b\ ^1\Sigma_g^+ \rightarrow X\ ^3\Sigma_g^-)$ atmospheric-oxygen band at 762 nm, both of which are excited in three-body O-atom recombination,[38,39] and also, in the case of $O(^1S)$, in the transfer of $N_2O(A\ ^3\Sigma_u^+)$ to $O(^3P)$.[17] Atomic-nitrogen recombination produces the $N_2(A)$. A final feature of Figure 5 is some argon lines to the red of 700 nm that are scattered from the discharge.

---

36. Young, R.A., and Sharpless, R.L. (1963) Chemiluminescent reactions involving atomic oxygen and nitrogen, J. Chem. Phys. 39:1071.

37. Groth, W., Kley, D., and Schurath, U. (1971) Rate constant for the infrared emission of the $NO(a\ ^4\Pi \rightarrow X\ ^2\Pi)$ transition, J. Quant. Spectrosc. Radiat. Transf. 11:1475.

38. Slanger, T.G., and Black, G. (1976) $O(^1S)$ production from oxygen atom recombination, J. Chem. Phys. 64:3767.
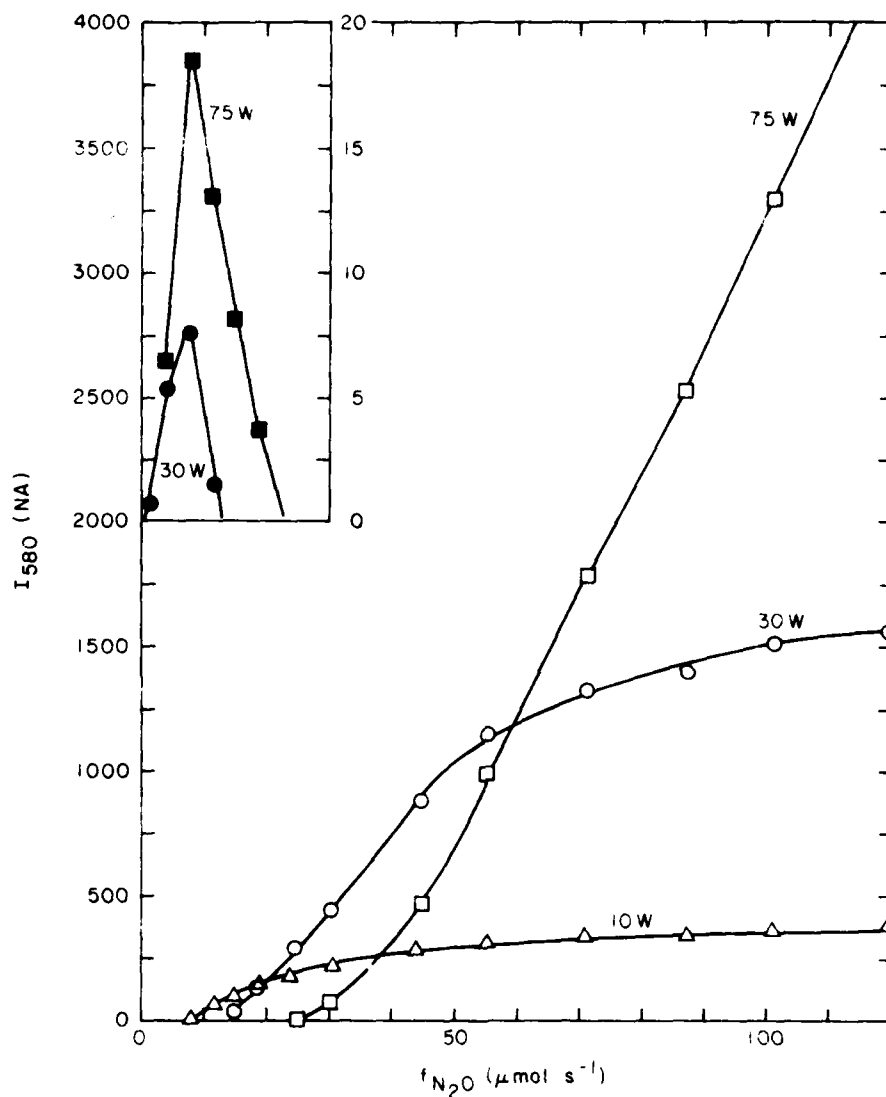
Figure 5. Variation in Emission Intensity at 580 nm From Ar/N₂O Discharge Products as a Function of N₂O Flow Rate. The inset shows intensity variations at low N₂O flow rates where the signal levels are two orders of magnitude below those at higher N₂O flow rates.
$f_{Ar} = 1395 \ \mu mol \ s^{-1}$, $p = 1.13$ Torr

Figure 4. Ultraviolet Spectrum Produced in N + O + Ar Recombination. $\Delta\lambda = 0.2$ nm. $f_{Ar} = 1470$ $\mu$mol s$^{-1}$, $f_{N_2O} = 21$ $\mu$mol s$^{-1}$, p = 1.18 Torr, power = 50 W



Figure 5. Nitrogen-atom Recombination Spectrum From Discharged $N_2O/Ar$. Argon lines scattered from the discharge appear at $\lambda > 700$ nm. $f_{Ar} = 4882$ $\mu$mol s$^{-1}$, $f_{N_2O} = 18$ $\mu$mol s$^{-1}$, p = 3.90 Torr, power = 50 W
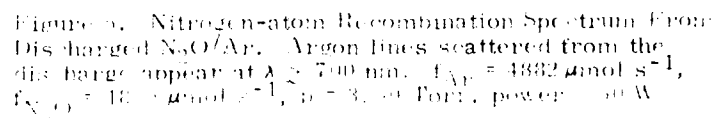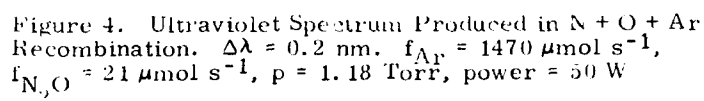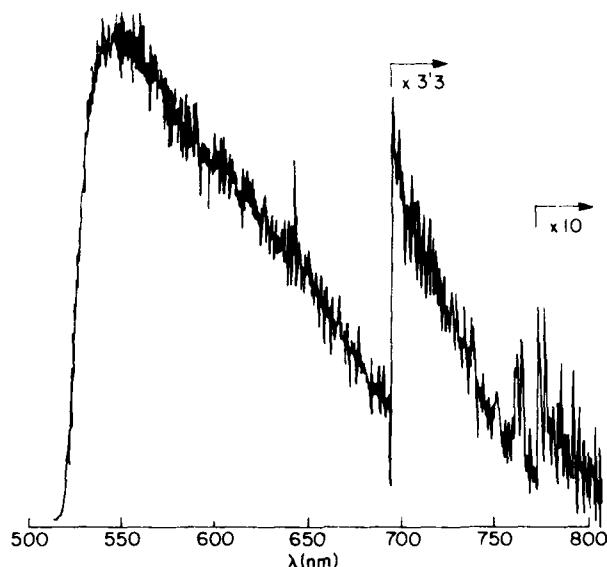
Figure 6. Air-afterglow Spectrum From Discharged
$N_2O/Ar$. The short wavelength limit is set by a
Corning 3-69 glass filter. $f_{Ar}$ = 4882 $\mu$mol s$^{-1}$,
$f_{N_2O}$ = 45 $\mu$mol s$^{-1}$, p = 3.50 Torr, power = 50 W

Figure 6 shows the continuum emission known as the air afterglow that results
from recombination of atomic oxygen and nitric oxide. The peculiar spectral dis-
tribution is caused by a Corning 3-69 colored glass filter that eliminates radiation
to the blue of 520 nm, and by the rapid decline of photomultiplier sensitivity at
longer wavelengths. The true air-afterglow spectral distribution declines only
25 percent between 600 and 800 nm.[22]

The preceding observations identify atomic nitrogen and atomic oxygen as
discharge products at low $N_2O$ flow rates. At high $N_2O$ flow rates nitric oxide
accompanies the atomic oxygen, and at intermediate $N_2O$ flow rates, the discharge
produces neither nitric oxide nor atomic nitrogen, only atomic oxygen. Figure 3
shows that this intermediate point where neither N nor NO is made, is a function
of discharge power, occurring at higher $N_2O$ flow rates when the discharge power
is higher. The initial peak in intensity at 580 nm, which is due to atomic-nitrogen
recombination is much more intense at higher discharge powers, indicating
greater N-atom production rates at higher powers. The dramatic increase in the
air-afterglow signal at higher discharge powers that is observed at high $N_2O$ flow
rates, shows that the higher-power discharges produce much more O and NO.

The plateaus for the 15-W discharge evident in Figure 3 at the higher $N_2O$ flow rates, and a similar one for data on a 20-W discharge that are not shown, corresponds to more than one-fourth of the available discharge power being used dissociating $N_2O$. The air-afterglow intensity at the plateau establishes the product $F_O F_{NO}$ through the calibration constant $\kappa$. The NO is formed through the reaction of $O(^1D)$ with $N_2O$ (see the following discussion) with a stoichiometry such that 1.33 mol of $O(^1D)$ are consumed to make 1 mol of NO.[39] To calculate a minimum required energy we assume that all atomic oxygen comes from a dissociation of $N_2O$ to $O(^3P)$ requiring 1.71 eV per molecule, and that the NO comes from dissociating $N_2O$ to $O(^1D)$ requiring 3.58 eV per molecule followed by its reaction with $N_2O$. These energies translate to minimum powers of 0.165 and 0.284 W needed to produce 1 $\mu$mol s$^{-1}$ of O and NO, respectively. The total minimum power for a given product effluent then is

$$P_{min} = 0.165\,F_O + 0.284\,F_{NO} \quad . \tag{9}$$

Knowing the product $F_O F_{NO}$ fixes one flow rate in terms of the other. Differentiating Eq. (9) with respect to the unknown flow rate and setting the result equal to zero establishes $P_{min} = 0.44\,(F_O F_{NO})^{1/2}$, where $P_{min}$ is in W and the flow rates are in $\mu$mol s$^{-1}$.

### 3.2 Quantitative Observations

Figure 7 shows the variation in the 580-nm emission intensity as a function of NO number density for several flow rates of $N_2O$ through a 30-W Ar/$N_2O$ discharge at 1.24 Torr. The slopes of these lines divided by the air-afterglow calibration constant, $\kappa$, determine the O-atom number densities for each $N_2O$ flow rate. The lines for the two lowest $N_2O$ flow rates have intercepts on the abscissa indicating that the discharge made atomic nitrogen in addition to the O-atoms. The other three lines all have intercepts on the ordinate showing that the product accompanying the atomic oxygen was nitric oxide. Figure 8 summarizes the data of Figure 7 by showing how the flow rates of O and N or NO out of the discharge vary with the flow rate of $N_2O$ into the discharge. At low $N_2O$ flow rates, the discharge converts approximately 75 percent of the $N_2O$ into atomic oxygen. Under similar conditions in our system, $Ar/O_2$ discharges convert only about 30 percent of the molecular oxygen to atoms, while $Ar/N_2$ discharges dissociate only about ___ percent of the molecular nitrogen.

___, ___, Bastie, D.R., Ridley, B.A., and Schiff, H.I. (1981) Measurements of the relative rate constants for the quenching of $O(^1D)$ atoms by $N_2O$ and $N_2$ and the branching ratio of the $N_2O$ reaction at 23 and -50 °C, J Phys Chem, ___.
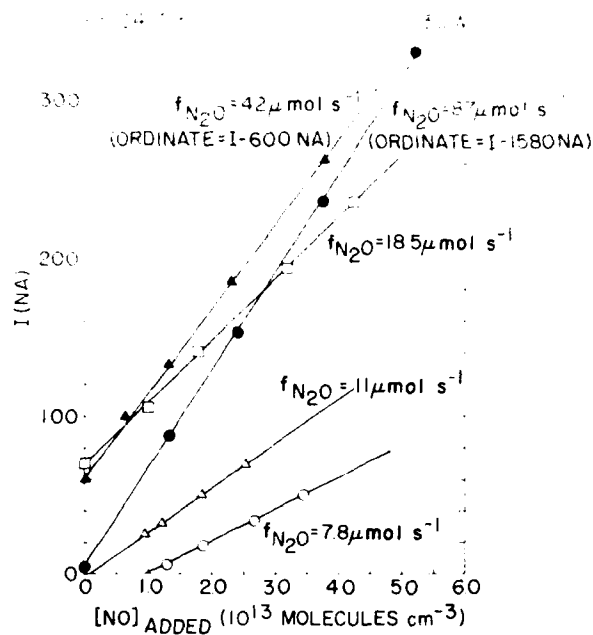
Figure 7. Intensity at 580 nm as a Function of
Added NO Number Density for Discharged
$N_2O/Ar$
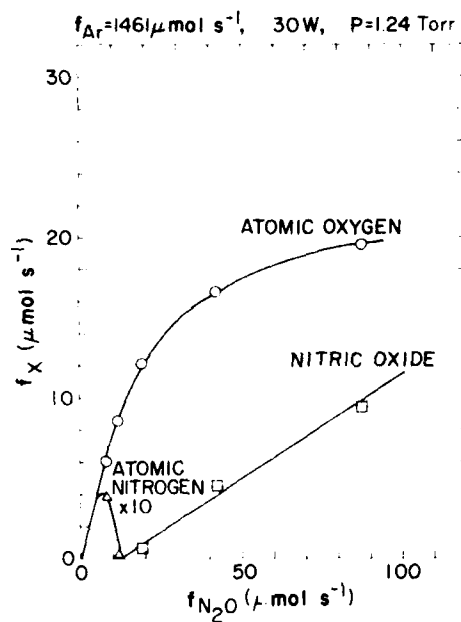


Figure 8. The Production of O, N, and NO
From $Ar/N_2O$ Discharges as a Function of
$N_2O$ Flow Rate

Atomic-nitrogen yields from the $Ar/N_2O$ discharges at low flow rates are generally 10 percent or less of those of atomic oxygen. Nitric oxide production at the higher $N_2O$ flow rates, on the other hand, approaches that of atomic oxygen under certain conditions. An additional interesting feature is that the product-NO flow rates appear to increase linearly as the $N_2O$ flow rate through the discharge is increased.

Figures 9 and 10 show how the O and NO products vary with $N_2O$ flow rate for two different argon flow rates at each of two different total pressures. We have omitted the appropriate atomic-nitrogen curves for clarity. The intercepts of the NO data indicate the transition point between N and NO production. These plots show that higher $Ar/N_2O$ mixing ratios suppress nitric oxide production, and that the onset of NO formation is delayed to higher $N_2O$ flow rates, and the efficiency of NO production as a function of $N_2O$ flow rate is smaller for larger flows of argon through the discharge. The slightly smaller O-atom production efficiency at the higher $N_2O$ flow rates in Figure 9 for the case of the large argon flow through the discharge probably results from a larger fraction of the available discharge power being taken up by the argon. The lower O-atom production efficiency of the low argon flow-rate case in Figure 10 probably results from enhanced wall recombination of the atomic oxygen at the lower pressures during the longer residence time in that discharge. Atomic-recombination wall efficiencies in active discharges often are on the order of 0.1 to 0.01,[40] large enough to make wall recombination a diffusion-controlled process.

Figure 11, in which the discharge residence time remains relatively constant, again shows the same trends in nitric oxide formation as a function of argon flow rate through the discharge as was shown in Figures 9 and 10 for the case of constant pressure.

Figure 12 shows that at constant argon flow rate, nitric oxide formation depends neither upon discharge residence time, nor pressure, thus reinforcing Figures 9 and 10 where the pressure was constant and Figure 11 where the residence times were similar. The differences in O-atom production efficiency in Figure 12 between the 0.42 and 1.24 Torr cases may not be significant. The maximum deviation of any pair of these data points from their average is only 3 per cent, and we do not anticipate a reproducibility between data taken under the same conditions but on different days to be any better than 10 percent. The lower O-atom production at the highest pressure probably results from chemical removal of O during the much longer residence times and at the higher number densities of reactive species in the discharge region.

40. Kaufman, F. (1969) The production of atoms and simple radicals in glow discharges, Advances in Chem. Ser. 80:29.
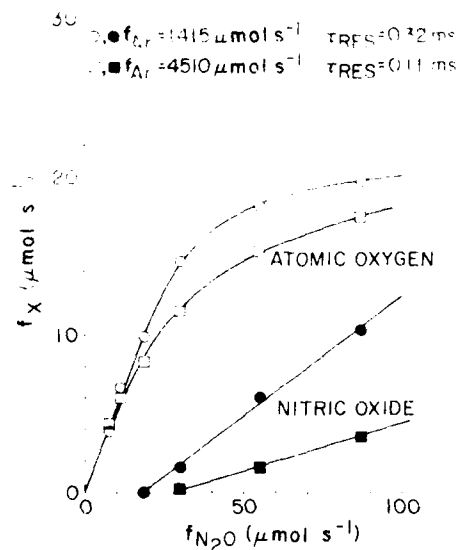
Figure 9. The Production of O and NO From Ar/$N_2$O Discharges as a Function of $N_2$O Flow Rate for Two Different Ar Flow Rates but Constant Pressure. P = 1.25 Torr, power = 30 W



Figure 10. The Production of O and NO From Ar/$N_2$O Discharges as a Function of $N_2$O Flow Rate for Two Different Ar Flow Rates but Constant Pressure. P = 0.2 Torr, power = 30 W

$\tau_{RES} = 0.37$ ms            30 W
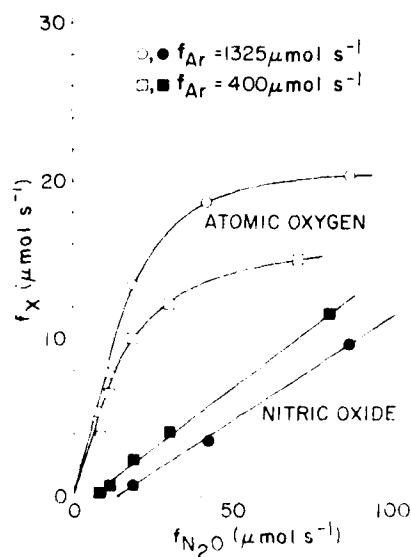
30

△,▲ $f_{Ar} = 400\ \mu$ mol s$^{-1}$    P=0.53 Torr

○,● $f_{Ar} = 1461\ \mu$ mol s$^{-1}$    P=1.24 Torr

□,■ $f_{Ar} = 4352\ \mu$ mol s$^{-1}$    P=3.1 Torr

ATOMIC OXYGEN

NITRIC OXIDE
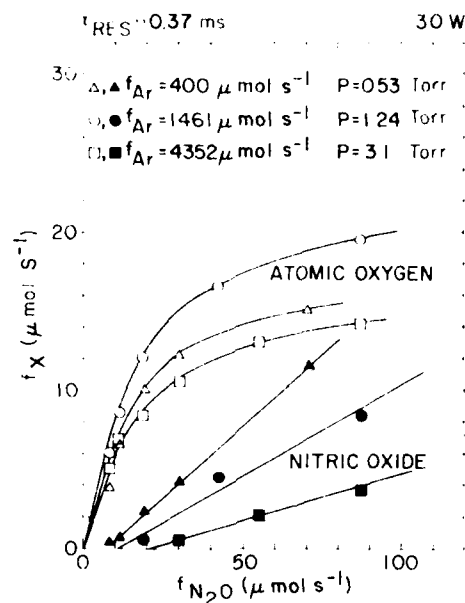
Figure 11. The Production of O and NO From
Ar/N$_2$O Discharges as a Function of N$_2$O Flow
Rate at Three Different Ar Flow Rates and
Pressures, but Similar Discharge Residence
Times



$f_{Ar} = 1400\ \mu$ mol s$^{-1}$           30 W

30

△,▲ P=0.52 Torr    $\tau_{RES} = 0.15$ ms

○,● P=1.24 Torr    $\tau_{RES} = 0.32$ ms

□,■ P=3.6 Torr    $\tau_{RES} = 0.98$ ms

ATOMIC OXYGEN

NITRIC OXIDE
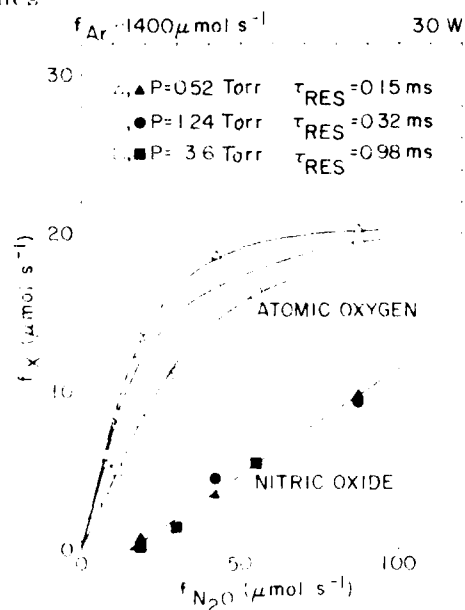
Figure 12. The Production of O and NO From
Ar/N$_2$O Discharges as a Function of N$_2$O Flow
Rate at Constant Ar Flow Rate but Varying
Pressures and Discharge Residence Times

Figure 13 compares the O and NO production from Ar/N$_2$O and He/N$_2$O discharges. The He/N$_2$O discharge produces nitric oxide at all N$_2$O flow rates, and in addition, is 25 to 30 percent less efficient as a source of atomic oxygen than is the Ar/N$_2$O discharge. This lower efficiency is consistent with our observations that the fractional O$_2$ dissociations in He/O$_2$ discharges are only about 20 to 25 percent in our system compared to the $\approx$ 30 percent fractional dissociation in an Ar/O$_2$ discharge. We discuss the differences between the Ar/N$_2$O and He/N$_2$O discharges further in the next section.

Adding molecular nitrogen to the discharge suppresses nitric-oxide formation, but at the expense of a reduced atomic-oxygen production efficiency. Figures 14, 15, and 16 demonstrate this point for cases of low, medium, and high initial nitric-oxide production efficiencies, respectively. For the case of low N$_2$O flow rate, fairly small flows of N$_2$ remove all the NO whereas, for the high N$_2$O flow-rate case, even when the N$_2$ comprises 30 percent of the total flow through the discharge, some of the NO remains. Even so, the nitric oxide product is reduced by almost two orders of magnitude while the atomic-oxygen effluent only is halved.

Figure 17 demonstrates that increased discharge power enhances significantly atomic-oxygen yields at the higher N$_2$O flow rates. At the low N$_2$O flow rates, the 30- and 50-W discharges produce O atoms from N$_2$O with equal efficiency.

$f_{Ar} = f_{He}$ 1475$\mu$mol s$^{-1}$, 30W, P=1.2 Torr
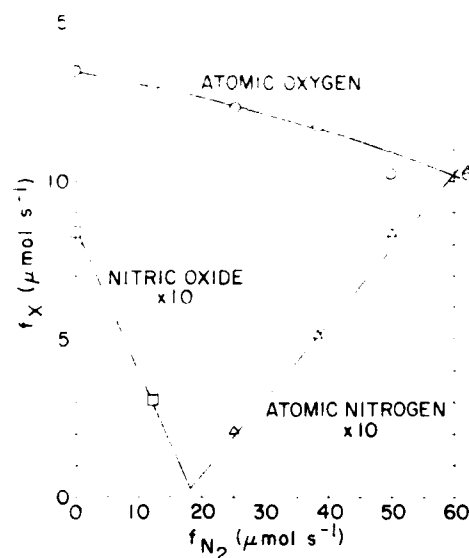
30

○,● Ar
□,■ He

20

ATOMIC OXYGEN
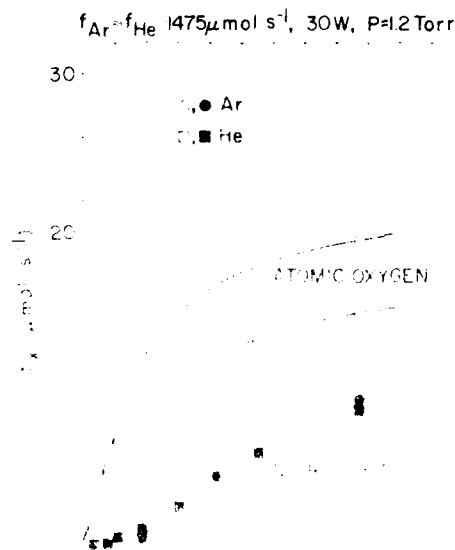
Figure 14. Variation in the Flow Rates of O, N, and NO Products From $Ar/N_2/N_2O$ Discharges as a Function of $N_2$ Flow Rate. $f_{Ar}$ = 1390 $\mu$mol s$^{-1}$, $f_{N_2O}$ = 18.5 $\mu$mol s$^{-1}$, p ≈ 1.25 Torr, power = 30 W

Figure 16. Variation in the Flow Rates of Atomic Oxygen and Nitric Oxide Products From $Ar/N_2/N_2O$ Discharges as a Function of $N_2$ Flow Rate. $f_{Ar} = 1405 \ \mu mol \ s^{-1}$, $f_{N_2O} = 87 \ \mu mol \ s^{-1}$, $p \approx 1.4$ Torr, power = 30 W



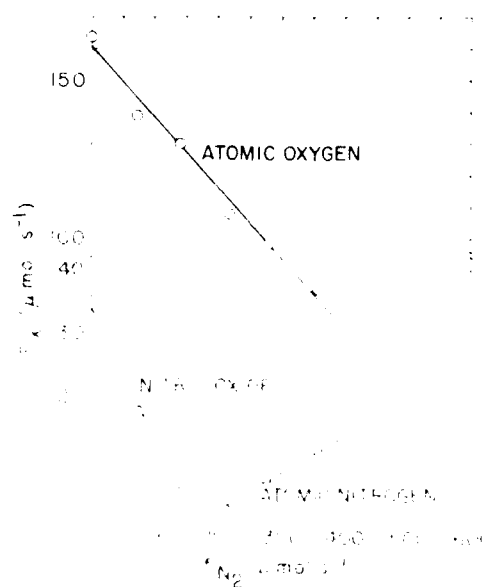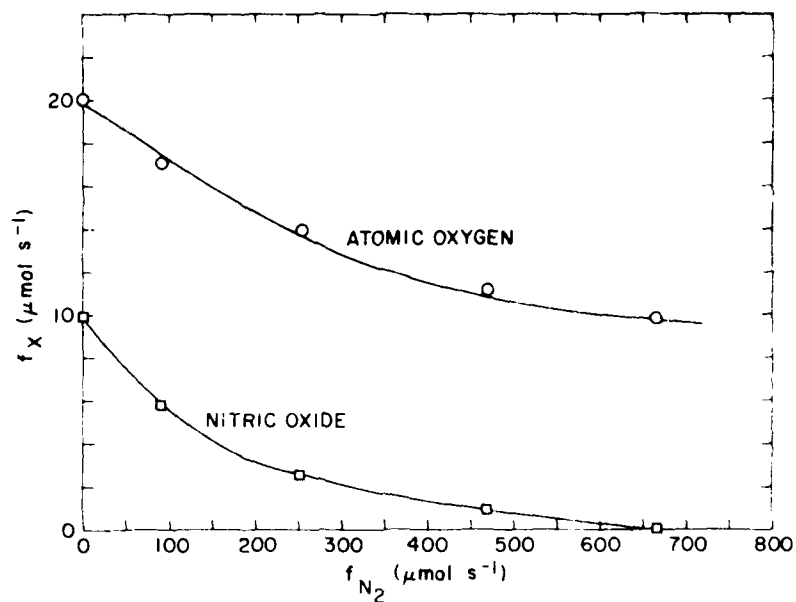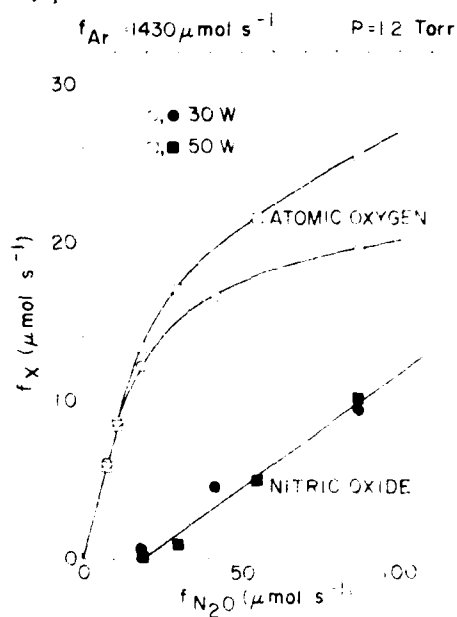Figure 17. The Production of O and NO From $Ar/N_2O$ Discharges as a Function of $N_2O$ Flow Rate at Two Different Discharge Powers

However, at the highest $N_2O$ flow rate studied, the 50-W discharge produces 30 percent more atomic oxygen than does the 30-W discharge. The apparent nitric oxide production efficiencies seem to be similar for the two different powers, although we know from the observations relating to Figure 3 that the higher power discharge requires higher $N_2O$ flow rates before NO-production commences.

## 4. KINETIC INTERPRETATIONS

Following Ung,[12] we expected $N_2O$ decomposition in a microwave discharge would occur primarily via the spin-allowed electron-impact dissociation pathway,

$$e^- + N_2O \rightarrow N_2 + O(^1D) + e^- \quad , \tag{10}$$

with the $O(^1D)$ rapidly quenched to $O(^3P)$ by Ar and wall collisions. The principal pathway for NO formation then would be reaction of $O(^1D)$ with $N_2O$:

$$O(^1D) + N_2O \rightarrow NO + NO \quad . \tag{11}$$

However, we could not explain N-atom production in the discharge, because N formation from electron-impact dissociation of $N_2O$, $N_2$, or NO should be too slow to compete with NO formed from Reaction (11). Furthermore, Reactions (10) and (11) would constitute a prolific source of NO, in contrast to our observation of $[O] \gg [NO]$. Thus, strictly qualitative arguments do not provide an obvious kinetic explanation of our results for $Ar/N_2O$ discharges.

We have developed and exercised a simple kinetic model, assuming typical (and somewhat idealized) discharge properties and surface recombination efficiencies, to provide a better understanding of the discharge kinetics. The model includes the major production and loss terms for each reagent, metastable intermediate, and product that are likely to contribute significantly to the observed results. The resulting rate equations are sufficiently coupled so as to require numerical solution by computer. The kinetic model shows that the decomposition of $N_2O$ by Reactions (10) and (11) fails to explain our observed O and NO yields, and indicates that the spin-forbidden process,

$$e^- + N_2O \rightarrow N_2 + O(^3P) + e^- \quad , \tag{12}$$

must form a substantial amount of O directly from $N_2O$. The dissociation of $N_2O$ by $Ar(^3P)$ metastables,

$$\text{Ar}^* + \text{N}_2\text{O} \rightarrow \text{N}_2(\text{B}\ ^3\Pi_g) + \text{O}(^3\text{P}) + \text{Ar} \quad , \tag{13}$$

appears to be another important pathway for O-atom production. Electron-impact dissociation of metastable $\text{N}_2$, primarily $\text{N}_2(\text{A}\ ^3\Sigma_u^+)$ formed by rapid cascade from $\text{N}_2(\text{B}\ ^3\Pi_g)$ produced in Reaction (13), is an important source of N at low initial $\text{N}_2\text{O}$ levels:

$$\text{e}^- + \text{N}_2^* \rightarrow \text{N} + \text{N} + \text{e} \quad . \tag{14}$$

The next sections describe the final kinetic model, the choice of rate parameters for the calculations, and the kinetic interpretations of the data base that the modeling implies. The kinetic modeling in this context substantiates mechanistic interpretations of the experimental data. It does not determine ab-initio quantitative rate coefficients or species concentrations, nor can it. However, the results of the modeling can give reasonable estimates of the magnitudes of concentrations of species not observed directly in the experiments.

### 4.1 Choice of Reactions and Rate Coefficients

Figure 18 illustrates the flow of chemical processes in our model; Table 1 lists important reactions and their rate coefficients. In this table, $\text{Ar}^*$ denotes, collectively, the $^3\text{P}_0$ and $^3\text{P}_2$ metastable states of argon, and $\text{N}_2^*$ denotes metastable $\text{N}_2(\text{A}\ ^3\Sigma_u^+)$ as formed by rapid cascade from the higher electronic states that are the actual initial products of the reactions. Some of the $\text{N}_2^*$ removal rate coefficients incorporate the possibility of vibrational excitation. Rate coefficients for the neutral bimolecular reactions come from information available in the literature with no further adjustments.

Electron-impact and surface removal processes govern the production and loss terms for critical species such as $\text{O}(^1\text{D})$, $\text{Ar}^*$, and $\text{N}_2^*$. The rate parameters for these processes are difficult to estimate to better than an order of magnitude because they are strong functions of conditions in the discharge. The absence of dissociation cross-section data for $\text{N}_2\text{O}$ and $\text{N}_2^*$ further compounds this problem. While we can estimate coefficients for the surface-removal processes fairly reliably from diffusion arguments and previous observations, we must rely on intuition to estimate the electron-impact coefficients based on knowing energy thresholds, cross sections for the desired species or similar molecules, and electron-energy distributions normally obtained in such discharges. Kaufman[40] has discussed these considerations in some detail and we implement the same principles here. We assume typical discharge conditions $P \sim 1$ Torr,

| Reaction | Net (Adopted) Rate Coefficient | Source |
|---|---|---|
| **$N_2O$ Reactions** | | |
| $e + N_2O \rightarrow O(^1D) + N_2 + e$ | | See text |
| $\rightarrow O(^3P) + N_2 + e$ | $1 \times 10^{-9}$ | Discharge estimate |
| $\rightarrow N + NO + e$ | $1 \times 10^{-10}$ | Discharge estimate |
| **$O(^1D)$ Reactions** | | |
| $O(^1D) + N_2O \rightarrow NO + NO$ | $7.2 \times 10^{-11}$ | a,b |
| $\rightarrow N_2 + O_2$ | $1.8 \times 10^{-11}$ | a,b |
| $O(^1D) + Ar \rightarrow O(^3P) + Ar$ | $3 \times 10^{-13}$ | a |
| $O(^1D) + N_2 \rightarrow O(^3P) + N_2$ | $3 \times 10^{-11}$ | a |
| $O(^1D) + NO \rightarrow O(^3P) + NO$ | $1.5 \times 10^{-10}$ | c |
| $O(^1D) + wall \rightarrow O(^3P)$ | $8 \times 10^3$ | Diffusion estimate |
| **Ar Metastable Reactions** | | |
| $Ar^* + e \rightarrow Ar + e$ | $1 \times 10^{-10}$ | Optimized – see text |
| $Ar^* + N_2O \rightarrow N_2 + O(^3P) + Ar$ | $4.4 \times 10^{-10}$ | d |
| $Ar^* + N_2 \rightarrow Ar + N_2$ | $3 \times 10^{-11}$ | d |
| $Ar^* + NO \rightarrow Ar + N + O(^3P)$ | $1.5 \times 10^{-10}$ | d |
| $Ar^* + O_2 \rightarrow Ar + O(^3P) + O(^3P)$ | $2 \times 10^{-10}$ | d |
| $Ar^* + O \rightarrow Ar + O$ | $8 \times 10^{-11}$ | e |
| $Ar^* + N \rightarrow Ar + N$ | $1.5 \times 10^{-10}$ | f |
| $Ar^* \rightarrow Ar$ | $1 \times 10^5$ | Optimized – see text |
| **$N_2$ Metastable Reactions** | | |
| $N_2^* + e \rightarrow N + N + e$ | $1 \times 10^{-8}$ | Discharge estimate |
| $N_2^* + Ar \rightarrow N_2 + Ar$ | $7 \times 10^{-15}$ | g |
| $N_2^* + N_2O \rightarrow N_2 + N_2 + O(^3P)$ | $6 \times 10^{-12}$ | h |
| $N_2^* + O \rightarrow N_2 + O$ | $3 \times 10^{-11}$ | i |
| $N_2^* + N \rightarrow N_2 + N$ | $5 \times 10^{-11}$ | j |
| $N_2^* + wall \rightarrow N_2$ | $6 \times 10^3$ | Diffusion estimate |
| **$N_2O$ Reactions** | | |
| $O(^3P) + e \rightarrow O(^1D) + e$ | $1 \times 10^{-8}$ | Discharge estimate |
| $O(^3P) + wall \rightarrow 1/2\ O_2$ | $5 \times 10^2$ | Diffusion estimate |
| $e + N_2 \rightarrow N + N + e$ | $1 \times 10^{-10}$ | Discharge estimate |
| $N + wall \rightarrow 1/2\ N_2$ | $5 \times 10^2$ | Diffusion estimate |
| $N + NO \rightarrow N_2 + O(^3P)$ | $3 \times 10^{-11}$ | k |

Rate coefficients are in units of $cm^3$ molecule$^{-1}$ s$^{-1}$ for bimolecular reactions and s$^{-1}$ for first-order surface deactivation/recombination processes.

References for Table 1

a. Schofield, K. (1978) Rate constants for the gaseous interactions $O(2\ ^1D_2)$ and $O(2\ ^1S_0)$ - A critical evaluation, J. Photochem. 9:55.

b. Lam, L., Hastie, D.R., Ridley, B.A., and Schiff, H.I. (1981) Measurements of the relative rate constants for the quenching of $O(^1D)$ atoms by $N_2O$ and $N_2$ and the branching ratio of the $N_2O$ reaction at 23 and -60°C, J. Photochem. 15:119.

c. McEwan, M.J., and Phillips, L.F. (1975) Chemistry of the Atmosphere, John Wiley & Sons, New York, p. 138.

d. Piper, L.G., Velazco, J.E., and Setser, D.W. (1973) Quenching cross sections for electronic energy transfer reactions between metastable argon atoms and noble gases and small molecules, J. Chem. Phys. 59:3323.

e. Piper, L.G., Clyne, M.A.A., and Monkhouse, P.B. (1982) Electronic energy transfer between metastable argon atoms and ground-state oxygen atoms, J. Chem. Soc., Faraday Trans. II 78:1373.

f. Piper, L.G., Clyne, M.A.A., and Monkhouse, P.B. (1980) Electronic energy transfer from metastable argon atoms to ground-state nitrogen atoms, Chem. Phys. 51:107.

g. Dreyer, J.W., and Perner, D. (1973) Deactivation of $N_2(A\ ^3\Sigma_u^+,\ v=0-7)$ by ground state nitrogen, ethane, and ethylene measured by kinetic absorption spectroscopy, J. Chem. Phys. 58:1195.

h. Clark, W.G., and Setser, D.W. (1980) Energy transfer reactions of $N_2(A\ ^3\Sigma_u^+)$. 5. Quenching by hydrogen halides, methyl halides, and other molecules, J. Phys. Chem. 84:2225.

i. Piper, L.G., Caledonia, G.E., and Kennealy, J.P. (1981) Rate constants for deactivation of $N_2(A\ ^3\Sigma_u^+, v'=0, 1)$ by O, J. Chem. Phys. 75:2847.

j. Dunn, O.J., and Young, R.A. (1976) Quenching of $N_2(A\ ^3\Sigma_u^+)$ by $O_2$, O, N, and H, Int. J. Chem. Kinet. 8:161.

k. Cheah, C.T., and Clyne, M.A.A. (1980) Reactions forming electronically-excited free radicals, J. Chem. Soc. Faraday II 76:1545.

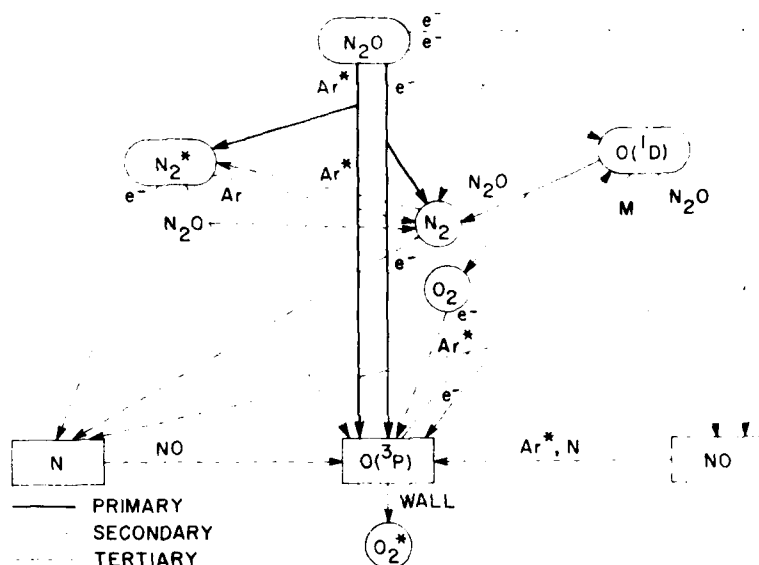Figure 18.  Reaction Pathways for $N_2O/Ar$
Discharge

$T \sim 500$ K, $E/N \sim 10^{-16}$ V $cm^2$, average electron energy $\sim 2$-3 eV, and primary electron density $\sim 3 \times 10^{11}$ $cm^{-3}$, with uniform properties along the entire length of the active discharge.

The dissociation of $N_2O$ by electrons can proceed by three possible pathways, forming $O(^3P)$, $O(^1D)$, or NO.  The N-NO branch has the largest energy threshold [4.93 eV as opposed to 1.68 eV for $N_2$-$O(^3P)$ and 3.66 eV for $N_2$-$O(^1D)$][41] and should be unimportant.  $O(^1D)$ is a critical precursor to NO through its reaction with $N_2O$.  Thus, the predicted NO yields are extremely sensitive to the extent of $O(^1D)$ production (see the following discussion).  $O(^1D)$ also is formed from electron-impact excitation of $O(^3P)$ and is collisionally quenched to $O(^3P)$ by a number of species in the discharge.  For these reasons, the $N_2O$ dissociation branching ratio is the most critical parameter in determining the O/NO ratio obtained on the discharge.

One branch of the $O(^1D) + N_2O$ reaction forms significant amounts of $N_2$ and $O_2$, but the bulk of the $N_2$ formed arises from $N_2O$ dissociation.  In gas mixtures containing Ar, the reaction between Ar metastables and $N_2O$ provides a direct

41.  Stull, D. R., and Prophet, H. (1971) JANAF Thermochemical Tables, Nat'l. Stand. Ref. Ser., NBS 37.

_____ _____ P_ ___ ____ _ the _____ ___ __ _____ __ ____ ___ ___ ___ N. The dissociation of $N_2$ by primary electrons proceeds below its very large rate coefficient,[42] so that this process should compete with the N-NO dissociation channel of $N_2O$ as a source of atomic nitrogen. In gas mixtures containing He, the interaction between He metastables and $N_2O$ leads primarily to Penning ionization,[44] followed by surface recombination of $N_2O^+$ and/or dissociative recombination with secondary electrons to give atomic oxygen; in this case, $N_2$ is not important and N may not be formed at significant levels.

We estimated first-order surface removal rates for $O(^1D)$ and $N_2$ by assuming unit deactivation probability and using the diffusion equation $k = (2.4/r)^2 D/P (T/300)^{3/2}$, where r is the radius of the discharge tube, D is the diffusion coefficient in $cm^2 s^{-1}$ at 1 Torr and 300 K, P is the pressure in Torr, and T is the temperature. Diffusion coefficients for $O(^1D)/Ar$[45] and $N_2/Ar$[46] are in the literature. Our previous observations of atomic concentrations in partially self-reversed discharge resonance lamps allowed us the estimate recombination coefficients for $O(^3P)$ and N.[47,48] These species do not appear to exhibit unit recombination efficiency, even in active discharges.

The kinetics of Ar discharges are somewhat complicated,[49] and representation of the $Ar^*$ formation and removal processes presents a special problem. We have chosen to express Ar production and loss in a shorthand form using direct

42. Gundell, L.A., Setser, D.W., Clyne, M.A.A., Coxon, J.A., and Nip, W.S. (1976) Rate constants for specific product channels from metastable $Ar(^3P_{0,2})$ reactions and spectrometer calibration in the vacuum ultraviolet, J. Chem. Phys. 64:4390.

43. Zipf, E.C. (1982) Ionization and dissociative excitation of $N_2$ by electron-impact on the metastable $N_2(A^3\Sigma_u^+)$ state, Bull. Am. Phys. Soc. 27:109.

44. Biola, J.P., Howard, J.S., Rundel, R.D., and Stebbings, R.F. (1974) Chemionization reactions involving metastable helium atoms, J. Phys. B 7:977.

45. Corney, A., and Williams, O.M. (1972) Measurement of the radiative lifetime of the $^1S_0$ metastable level of atomic oxygen, J. Phys. B 5:686.

46. Levron, D., and Phelps, A.V. (1978) Quenching of $N_2(A^3\Sigma_u^+, v=0, 1)$ by $N_2$, Ar, and $H_2$, J. Chem. Phys. 69:2260.

47. Rawlins, W.T., and Kaufman, F. (1977) Characteristics of O(I) and N(I) resonance line broadening in low pressure helium discharge lamps, J. Quant. Spectrosc. Radiat. Trans. 18:561.

48. Rawlins, W.T. (1977) Applications of OI and NI Resonance Absorption in the Vacuum Ultraviolet to Studies of Electronic Energy Transfer in Active Nitrogen, Line Broadening in Low Pressure He Discharge Lamps, and Thermospheric $O(^3P)$ and $N(^4S)$ Densities, Thesis, University of Pittsburgh.

49. Delcroix, J.L., Ferreira, C.M., and Ricard, A. (1975) Atomic and Molecular Metastables in the Electrical Discharge, University of Paris-South.

electron-impact excitation and an effective first-order removal that is consistent with other observations in the active discharge. In previous observations of atomic-nitrogen resonance radiation excited by direct energy transfer from $Ar^*$ in a nearly-pure Ar discharge, we noted that the addition to the active discharge of significant amounts of Xe, a strong quencher of $Ar^*$, reduced the steady-state number density of $Ar^*$ only moderately, implying that the net loss rate for $Ar^*$ must be near $10^5$ $s^{-1}$ in pure Ar.[18,50] (This effect could be due largely to quenching of $Ar^*$ by secondary electrons.[49]) Using this value to describe $Ar^*$ removal, we then adjusted the $Ar^*$ production coefficient to give a large enough $Ar^*$ number density to match the observed N and O yields as described here. The resulting rate coefficient is consistent with a pure Ar discharge but is about a factor of 10 greater than we might expect for Ar with impurity levels of a few percent. However, we have not considered other $Ar^*$ sources (for example, cascade from higher states formed in dissociative recombination of $Ar_2^+$ with electrons), and our assumed electron density may be too small. In any case, the relevant factor is the steady-state $Ar^*$ number density that is in the $10^{12}$ $cm^{-3}$ range, consistent with Ar and He metastable number densities required to explain flux levels of O and N resonance radiation observed in microwave-discharge line sources.[18,47,48,50] Furthermore, the predicted $Ar^*$ number density is only weakly dependent on the initial $N_2O$ concentration, as we previously observed for Xe as a collision partner.[18,50] This latter effect is important for our analysis, because $e^- + N_2O$ is not sufficient by itself to explain our observed $[O]/[NO]$ ratios, and we require that 20 to 50 percent of the early-time O production take place via $Ar^* + N_2O$ over a 20-fold variation in $[N_2O]_0$.

## 4.2 Results of Calculations

The calculations used a modified predictor-corrector computer code designed to solve numerically "stiff" systems of coupled differential equations.[51] Time-dependent solutions extend 500 $\mu s$, typical residence times in our discharges are ~300 $\mu s$. Figure 19 shows sample results for an $Ar/N_2O$ mixture. At about 200 $\mu s$, the kinetics are nearly in steady-state. Figure 20 displays the species concentrations as functions of initial $N_2O$ level at 300 $\mu s$, representative of the neutral gas composition at the exit of the active discharge.

50. Piper, L.G., Murphy, H.C., and Rawlins, W. T. (1981) Development of COCHISE UV Absorption System, Final Report, AFGL-TR-81-0318. AD A111828.

51. Lewis, P. F. (1971) The Forward Marching Solution of Coupled Differential Equations, Physical Sciences Inc., TR-19.
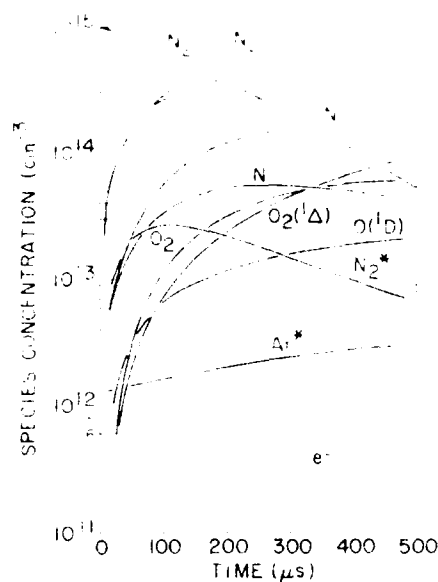
Figure 19. Predicted Species Evolution in an Ar/N₂O Microwave Discharge Plasma, Using the Reaction Set of Table 1. [Ar] = 2.4 × 10¹⁷ cm⁻³, [N₂O]₀ = 1 × 10¹⁵ cm⁻³
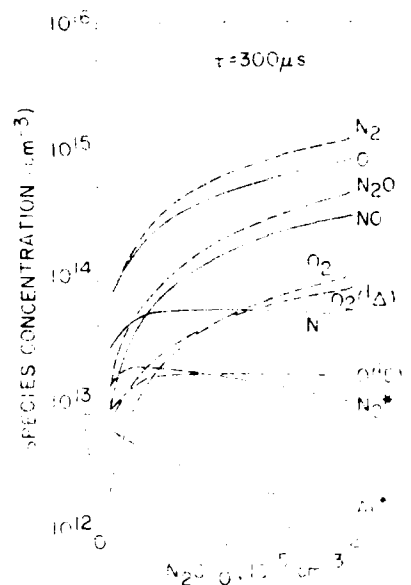


Figure 20. Predicted Species Concentrations at Discharge Exit (600 μs) as Functions of Initial N₂O Concentrations, Using the Reaction Set of Table 1 and [Ar] = 2.4 × 10¹⁷ cm⁻³

Since the actual measurements of O, N, and NO are made some distance downstream from the discharge, we must correct the predicted concentrations because the reaction

$$N + NO \rightarrow N_2 + O \tag{13}$$

proceeds to completion between the discharge exit and the measurement station. Figure 21 compares the final, predicted concentrations of O, N, and NO at the measurement port as functions of $[N_2O]_0$ with experimental results obtained under comparable conditions. Figure 21 also indicates predictions for the case where $N_2O$ dissociation by electrons proceeds entirely via the $O(^1D)$ production channel [Reaction (10)] with a rate coefficient of $10^{-8}$ cm$^3$ s$^{-1}$. The $O(^3P)$ case clearly compares very nicely with the observations, while the $O(^1D)$ case gives too much NO and not enough O. More significantly, the predicted $[O]/[NO]$ ratio is inconsistent with experimental results. NO formation is overpredicted in the case where Reactions (10) and (11) are assumed, because at early times, before significant $N_2$ has built up, $N_2O$ is the major quenching partner for $O(^1D)$. In that case every three $N_2O$ molecules form two NO molecules but no $O(^3P)$. As $N_2$ and NO accumulate, this branching ratio moderates somewhat, but most of the NO has already been formed at this point. Increasing the rate of Reaction (10) by an order of magnitude increases [O] but does not change [NO]. Consuming $N_2O$ by electrons faster than the $O(^1D)$ can react with it requires an unreasonably large rate for Reaction (10).

Thus, direct production of $O(^3P)$ from $N_2O$ is necessary. Reacting $N_2O$ with Ar* provides such a source. If we reduce the rate of Reaction (10) to agree with experimental [NO] data, however, we obtain [O] < [NO], unless we postulate extraordinarily high [Ar*]. Therefore, we must conclude that, in a microwave discharge, the electron-impact dissociation of $N_2O$ proceeds primarily, if not entirely, by formation of $O(^3P)$ in a spin-forbidden process.

Comparison with data obtained for other gas mixtures at similar pressures, flow rates, and discharge powers (that is, comparable discharge conditions) strengthen our interpretations. Calculations on He/$N_2O$ mixtures use the mechanism of Table 1 except, of course, for the reactions involving Ar*. He* conceivably could lead to O formation via Penning ionization of $N_2O$ followed by dissociative recombination of electrons with $N_2O^+$ or, possibly, with $NO^+$, which would be formed by rapid charge exchange. However, this mechanism has many pitfalls: (1) He* is probably in somewhat lower concentration than Ar*, thus reducing the overall throughput; (2) $N_2O^+$ and $NO^+$ might be subject to other fast loss processes, such as surface recombination; (3) dissociative recombination will form electronically excited O or N which would in turn lead to the formation of NO rather
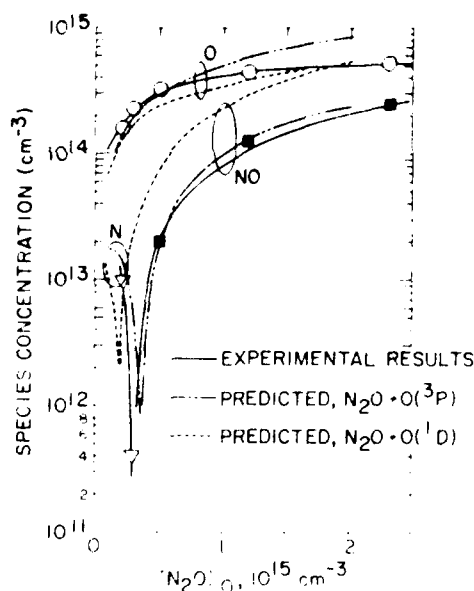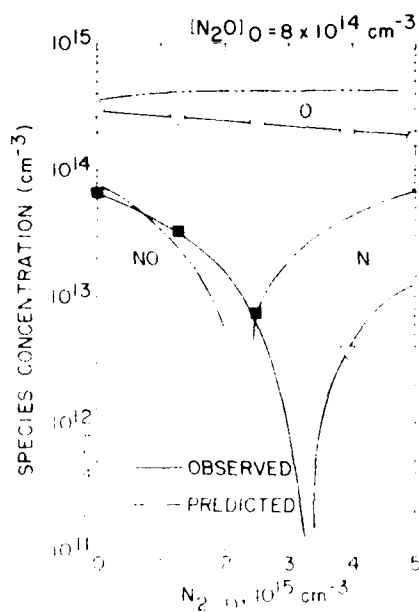
Figure 21. Experimental and Predicted
Concentrations of O, N, and NO at the
Measurement Station for an $Ar/N_2O$
Microwave Discharge. The solid curve
and points are the experimental data
from Figure 3.

than $O(^3P)$ [for example, $O(^1D) + N_2O$ or $N(^2P) + N_2O$]. In view of this complexity
and the likelihood that the overall contribution is less than 10 percent (that is,
much less than the $Ar^+ + N_2O$ channel), we have omitted the He kinetics in our
calculations. Figure 22 compares the predictions for the $He/N_2O$ and $Ar/N_2O$
cases. These predictions relate to the experimental observations shown in
Figure 13. In accord with the measurements, the calculations predict a 20 to
30 percent reduction in O production for $He/N_2O$ and production of NO at all $N_2O$
levels. We conclude that the observed reduced O yields result from the absence
of the $Ar^+ + N_2O$ reaction, and that the continuous production of NO results from
the absence of $Ar^+$, which virtually eliminates $N_2$, and thereby N atoms, the
major sink for NO.

Figure 25 shows the extension of the calculations to $Ar/N_2O/N_2$ mixtures.
Again, the calculations predict the general behavior observed in the experiments.
In this case, we greatly overpredict the N production, undoubtedly because the
assumed rate coefficient for dissociation of $N_2$ by electrons is too large. While
this process is insignificant for $Ar/N_2O$ mixtures, it is the main source of N for
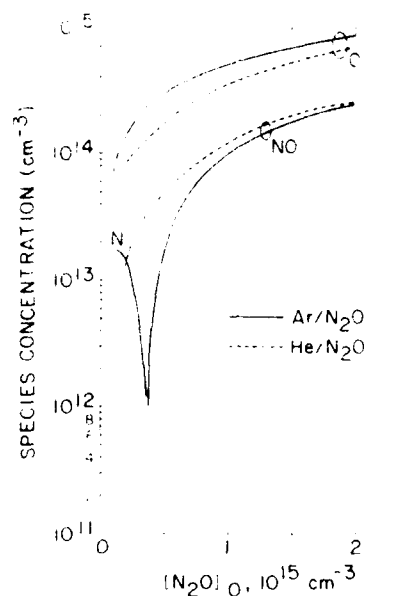
Figure 22. Predicted Concentrations of O, N, and NO at the Measurement Station for Ar/N$_2$O and He/N$_2$O Microwave Discharge



Figure 23. Experimental and Predicted Concentrations of O, N, and NO at the Measurement Station for an Ar/N$_2$/N$_2$O Microwave Discharge. [N$_2$O]$_0$ = 8 $\times$ 10$^{17}$ cm$^{-3}$. The experimental data are from Figure 1.

this case. Furthermore, the addition of such large amounts of $N_2$ to the discharge will alter the characteristic electron energy distribution and number density significantly, and might render kinetic processes involving atomic-nitrogen metastables significant, although still minor. We considered neither of these factors The important point, however, is that fairly large amounts of $N_2$ are required to produce enough N to remove the NO that is formed in Reaction (11).

## 5. SUMMARY AND CONCLUSIONS

The experimental results show that $Ar/N_2O$ discharges are indeed prolific sources of atomic oxygen. We were able to generate O-atom flows over 2 $\mu$mol s$^{-1}$ at fairly modest discharge powers. The source is also very efficient, converting about 75 percent of the nitrous oxide to atomic oxygen at nitrous-oxide feed rates less than 10 to 20 $\mu$mol s$^{-1}$. Judicious manipulation of discharge power, and the addition of molecular nitrogen to the discharge prevents atomic-nitrogen or nitric oxide from accompanying the atomic oxygen product. The point at which atomic nitrogen and nitric oxide both are absent is indicated readily by the absence of emission of 580 nm, N-atom and O/NO recombination both being strong sources of 580-nm emission.

The modeling calculations reproduce the experimental results reasonably well under the assumptions that the electron-impact dissociation of $N_2O$ proceeds through the spin-forbidden channel to produce $O(^3P)$, and that about 20 percent of the dissociations result from collisions between metastable argon atoms and $N_2O$. The modeling calculations also indicate that perhaps as much as 5 percent of the nitrous oxide fed to the discharge is undissociated, and that the molecular oxygen flow rates out of the discharge are generally an order of magnitude less than those of atomic oxygen. Thus, the argon/nitrous oxide discharge can be a relatively clean source of atomic oxygen with only minor amounts of atomic nitrogen, nitric oxide, or molecular oxygen accompanying the O-atoms out of the discharge region, with the two former products being controllable to some extent.

# References

1. Howard, C.J. (1979) Kinetic measurements using flow tubes, _J. Phys. Chem._ 83:3.

2. Elias, L., Ogryzlo, E.A., and Schiff, H.I. (1959) The study of electrically discharged $O_2$ by means of an isothermal calorimetric detector, _Can. J. Chem._ 37:1680.

3. Mathias, A., and Schiff, H.I. (1964) _Discussions Faraday Soc._ 37:38.

4. March, R.E., Furnival, S.G., and Schiff, H.I. (1965) _Photochem. Photobiol._ 4:971.

5. Cook, T.J., and Miller, T.A. (1974) Production of $^1\Delta_g$ $O_2$ from microwave discharges in $CO_2$, $NO_2$ and $SO_2$, _Chem. Phys. Lett._ 25:396.

6. Piper, L.G. (1978) Unpublished results.

7. Kaufman, F., and Kelso, J.R. (1958) _Reactions of Atomic Oxygen and Atomic Nitrogen With Oxides of Nitrogen_, 7th Int. Symp. Combustion, p. 53.

8. Black, G., and Slanger, T.G. (1981) Production of $O_2(a\ ^1\Delta_g)$ by oxygen atom recombination on a Pryex $^R$ surface, _J. Chem. Phys._ 74:6517.

9. Lundell, O.R., Ketcheson, R.D., and Schiff, H.I. (1969) _The Production of $O(^3P)$ Atoms, Free From Excited Molecules, and Their Reaction With $O_3$_, 12th Int. Symp. Combustion, p. 307.

10. McCrumb, J.L., and Kaufman, F. (1972) Kinetics of the $O + O_3$ reaction, _J. Chem. Phys._ 57:1270.

11. Rawlins, W.T., Piper, L.G., Caledonia, G.E., and Green, B.D. (1981) _COCHISE Research_, Physical Sciences Inc., TR-298.

12. Ung, A.Y.M. (1975) A microwave discharge in $N_2O-N_2$ mixtures: A prolific source of oxygen atoms, _Chem. Phys. Lett._ 32:351.

13. Kaufman, F. (1958) The air afterglow and its use in the study of some reactions of atomic oxygen, _Proc. Roy. Soc. (London)_ 247A:123.

16. Piper, L.G., Calcdone, G.E., and Bremaier, J.P. (1985) Rate constants for deactivation of $N_2(A\ ^3\Sigma_u^+, v'=0, 1)$ by O. J. Chem. Phys. 75:2847.

17. Piper, L.G. (1982) The excitation of O($^1$S) in the reaction between $N_2(A\ ^3\Sigma_u^+)$ and O($^3$P), J. Chem. Phys. 77:2373.

18. Rawlins, W.T., and Piper, L.G. (1981) Effects of excitation mechanism on linewidth parameters of conventional vacuum ultraviolet (VUV) discharge line sources, Proc. Soc. Photo.-Opt. Instrum. Eng. 279:58.

19. Piper, L.G., Clyne, M.A.A., and Monkhouse, P.B. (1982) Electronic energy transfer between metastable argon atoms and ground-state oxygen atoms, J. Chem. Soc. Faraday Trans. II 79:1373.

20. Borg, H.C., and Kleppner, D. (1962) Rev. Sci. Instr. 33:248.

21. Golde, M.F., and Thrush, B.A. (1973) Afterglows, Rep. Prog. Phys. 36:1265.

22. Fontijn, A., Meyer, C.B., and Schiff, H.I. (1964) Absolute quantum yield measurements of the NO - O reaction and its use as a standard for chemiluminescent reactions, J. Chem. Phys. 40:64.

23. Sutoh, M., Morioka, Y., and Nakamura, M. (1980) Absolute rate constant for the chemiluminescent reaction of atomic oxygen with nitric oxide, J. Chem. Phys. 72:20.

24. Clough, P.N., and Thrush, B.A. (1967) Mechanism of the chemiluminescent reaction between nitric oxide and ozone, Trans. Faraday Soc. 63:915.

25. McCarroll, B. (1970) An improved microwave discharge cavity for 2450 MHz, Rev. Sci. Instr. 41:279.

26. Manson, D. (1982) Matheson Gas Co., Gloucester, Mass. Private communication to L.G. Piper.

27. Vanpee, M., Hill, K.D., and Kineyko, W.R. (1971) Absolute rate constant measurements for the radiative combination of atomic oxygen with nitric oxide, AIAA J. 9:135.

28. Golde, M.F., Roche, A.E., and Kaufman, F. (1973) Absolute rate constant for the O + NO chemiluminescence in the near infrared, J. Chem. Phys. 59:3953.

29. Golomb, D., and Brown, J.H. (1975) The temperature dependence of the NO - O chemiluminous recombination. The RMC mechanism, J. Chem. Phys. 63:5246; AFCRL-TR-76-0036, AD A020761.

30. Woolsey, G.A., Lee, P.H., and Slater, W.D. (1977) Measurement of the rate constant for NO - O chemiluminescence using a calibrated piston source of light, J. Chem. Phys. 67:1220.

31. Pravilov, A.M., and Smirnova, L.G. (1978) Spectral distribution of the chemiluminescence rate constant in the O + CO(+M) and O + NO(+He) reactions, Kinet. and Catal. 19:202.

32. Husain, D., and Slater, N.K.H. (1980) Kinetic study of ground state atomic nitrogen, $N(2\ ^4S_{3/2})$ by time-resolved atomic resonance fluorescence, J. Chem. Soc. Faraday Trans. II 76:606.

33. Lee, J.H., Michael, J.V., Payne, A.... and Stief, L.J. (1978) ...
rate ... of N(²S) ... NO ... by ...
FP-RF techniques, J. Chem. Phys. 69:3069.

34. Clyne, M.A.A., and McDermid, I.S. (1975) Mass spectrometric determina-
tions of the rates of elementary reactions of N and N₂ with ground state
... J. Chem. Soc., Faraday Trans. ...

. Baulch, D.L., Drysdale, D.D., Horne, D.G., and ...
Evaluated Kinetic Data for High Temperature Reaction. II. Homogeneous
Gas Phase Reactions of the H₂ - N₂ - O₂ System, Butterworths, ... Eng.

35. Young, R.A., and Sharpless, R.L. (1963) Chemiluminescent reactions
involving atomic oxygen and nitrogen., J. Chem. Phys. 39:1071.

37. Groth, W., Kley, D., and Schurath, U. (1971) Rate constant for the infrared
emission of the NO(C ²Π → A ²Σ⁺) transition, J. Quant. Spectrosc.
Radiat. Trans. 11:1475.

38. Slanger, T.G., and Black, G. (1976) O(¹S) production from oxygen atom
recombination, J. Chem. Phys. 64:3767.

39. Lam, L., Hastie, D.R., Ridley, B.A., and Schiff, H.I. (1981) Measure-
ments of the relative rate constants for the quenching of O(¹D) atoms by
N₂O and N₂ and the branching ratio of the N₂O reaction at 25 and -60 °C,
J. Photochem. 15:119.

40. Kaufman, F. (1969) The production of atoms and simple radicals in glow
discharges, Advances in Chem. Ser. 80:29.

41. Stull, D.R., and Prophet, H. (1971) JANAF Thermochemical Tables,
Nat'l. Stand. Ref. Ser., NBS 37.

42. Gundel, L.A., Setser, D.W., Clyne, M.A.A., Coxon, J.A., and Nip, W.S.
(1976) Rate constants for specific product channels from metastable
Ar(³P₂,₀) reactions and spectrometer calibration in the vacuum ultra-
violet, J. Chem. Phys. 64:4390.

43. Zipf, E.C. (1982) Ionization and dissociative excitation of N₂ by electron-
impact on the metastable N₂(A ³Σ⁺ᵤ) state, Bull. Am. Phys. Soc. 27:100.

44. Riola, J.P., Howard, J.S., Rundel, R.D., and Stebbings, R.F. (1974)
Chemiionization reactions involving metastable helium atoms, J. Phys. B
7:376.

45. Corney, A., and Williams, O.M. (1972) Measurement of the radiative life-
time of the ¹Sₒ metastable level of atomic oxygen, J. Phys. B 5:686.

46. Levron, D., and Phelps, A.V. (1978) Quenching of N₂(A ³Σ⁺ᵤ, v=0, 1) by N₂,
Ar, and H₂, J. Chem. Phys. 69:2260.

47. Rawlins, W.T., and Kaufman, F. (1977) Characteristics of O(I) and N(I)
resonance line broadening in low pressure helium discharge lamps,
J. Quant. Spectrosc. Radiat. Trans. 18:561.

48. Rawlins, W.T. (1977) Applications of OI and NI Resonance Absorption in the
Vacuum Ultraviolet to Studies of Electronic Energy Transfer in Active
Nitrogen, Line Broadening in Low Pressure He Discharge Lamps, and
Thermospheric O(³P) and N(⁴S) Densities, Thesis, University of
Pittsburgh.

49. Delcroix, J.L., Ferreira, C.M., and Ricard, A. (1973) Atomic and
Molecular Metastables in the Electrical Discharges, University of Paris-
South.

50. Piper, L.G., Murphy, H.C., and Rawlins, W.T. (1981) Development of
COCHISE UV Absorption System, Final Report, AFGL-TR-81-0315,
AD A111826.

42

51. Lewis, P.F. (1974) <u>The Forward Marching Solution of Coupled Differential Equations</u>, Physical Sciences Inc., TR-19.

44

# Appendix A

## Application of $N_2O$ Discharges to COCHISE $O_3$ Studies

The recombination of atomic and molecular oxygen may give rise to vibrationally excited ozone in the upper atmosphere via the sequence:

$$O + O_2 + M \rightarrow O_3(v') + M \tag{A1}$$

$$O_3(v') + M \rightarrow O_3(v'') + M \tag{A2}$$

$$O_3(v') \rightarrow O_3(v'') + h\nu \tag{A3}$$

Recent rocketborne measurements[A1,A2] of infrared atmospheric emissions indicate that chemiluminescence in the $\nu_3$ fundamental band of $O_3$ [Reaction (A3)] may be a significant source of 10- to 12-$\mu$m radiation in the upper atmosphere between 90 and 100 km.

The COCHISE facility possesses a unique capability for the investigation of Reactions (A1) through (A3), owing to its high sensitivity near 10 $\mu$m. A

A1.  Nadile, R.M., Stair, A.T., Jr., Wheeler, N.B., Frodsham, D.G., Wyatt, C.L., Baker, D.J., and Griedler, W.F. (1978) SPIRE-Spectral Infrared Rocket Experiment (Preliminary Results), AFGL-TR-78-0107, AD A058504.

A2.  Green, B.D., Rawlins, W.T., and Caledonia, G.E. (1980) Interim Report on High Altitude Radiation Signatures, Physical Sciences Inc., TR-231.

preliminary investigation[A3-A5] of the recombination processes yielded the first laboratory spectra ever obtained of $O_3$ vibraluminescence. In these experiments, $O_2$/Ar mixtures (0.5 to 73 percent $O_2$) were passed through the microwave discharges to produce O. $O_2$ and Ar were alternately used as counterflow gases. The important findings of that study are: (1) most or all of the observed $O_3$ emission (limited to the $\nu_3$ band near 10 $\mu$m) was the net result of recombination and collisional deactivation [Reactions (A1) and (A2)] occurring in the discharge sidearms; (2) the observable steady-state vibrational populations under these conditions extended as high as v' ~ 6; and (3) the vibrational analysis was complicated by the possibility of excitation of the manifolds of the combination states $(\nu_1 + \nu_3)$ and $(\nu_2 + \nu_3)$. These results have been extended in more recent COCHISE experiments; these data and their aeronomic significance are discussed in detail in an earlier report.[A6]

Successful measurements of nascent $O_3(v)$ from Reaction (A1) in COCHISE will require (1) attainment of favorable pressure (controlled by the reaction cell temperature) and atomic oxygen concentration (controlled by the discharge conditions) in the flow interaction region of the reaction cell and (2) elimination of fluorescence contributions from $O_3(v)$ formed in the discharge inlet tubes. The experimental conditions required for the first goal can be mapped approximately for typical discharge operations by means of a steady-state analysis similar to that used in References A3 and A5. Briefly, $O_3(v)$, formed in the interaction zone by recombination of discharge-produced O with counterflowing $O_2$, is in steady state (while the discharges are on) between formation by Reaction (A1) and removal by both collisional relaxation and cryopumping to the cell wall. The collisional deactivation rate will be essentially that due to collisions between $O_3(v)$ and O,[A7] since other species likely to be present (such as $O_2$ and Ar) are relatively inefficient relaxation partners for $O_3(v)$.[A8,A9] The cryopumping rate is difficult to estimate due to uncertainties in the effective cryocapture coefficients and possible effects of wall collisions on species in the field-of-view; these uncertainties arise primarily at elevated cell pressure and temperature. Simple mass flow considerations[A10,A11] suggest a pumping rate of $1.4 \times 10^4/P_{mt}$ where $P_{mt}$ is the reaction zone pressure in mTorr. The results of this steady-state exercise for three cell pressures are shown in Figure A1. The effects of relaxation by atomic oxygen can be seen in the deviation of the solid curves from the dashed line. These feasibility estimates indicate that the most favorable conditions for observing nascent distributions are pressures near 10 mTorr and $[O]/[O_2]$ ratios near 0.01 to 0.1. By comparison, previous COCHISE $O_3(v)$ experiments[A5] were

---

Because of the large number of references cited above, they will not be listed here. See References, page
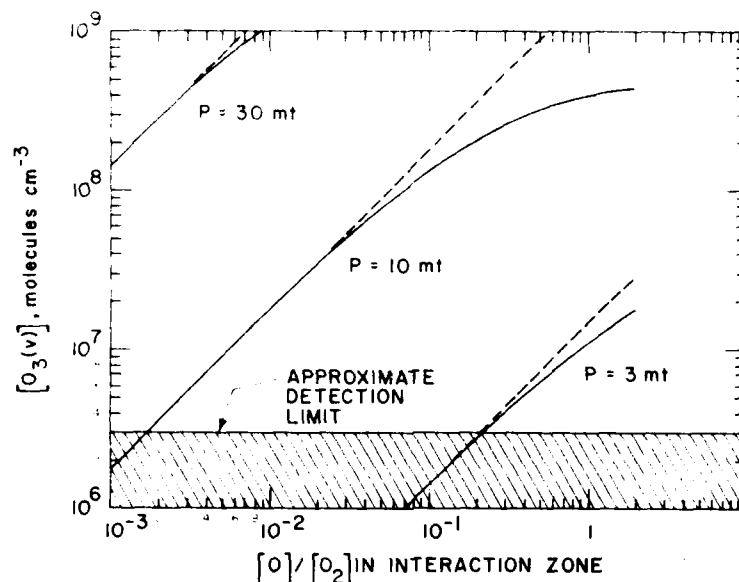
46

Figure A1. Anticipated $O_3(v)$ Yields in Interaction Zone for Discharge-flow of $Ar/N_2O$ vs $O_2$ Counterflow, 100 K. The difference between dashed and solid curves illustrates the effect of O vibrational quenching at high $[O]/[O_2]$

performed at 3 mTorr and $[O]/[O_2] < 0.01$. No evidence could be found of $O_3(v)$ formed in the flow interaction zone; this result is consistent with the prediction of Figure A1. We have since operated COCHISE at reaction zone pressures as high as 30 mTorr; however, further measurements at elevated pressures will be needed to characterize the operating conditions and effective residence times more fully.

In order to observe nascent $O_3(v)$ in the reaction volume, O must be generated such that recombination with $O_2$ in the discharge tubes is avoided. An attractive possible method is by microwave discharge of $N_2/N_2O/Ar$ mixtures, in which O can be generated in the near absence of $O_2$, as described in this report. This technique has also been demonstrated by Ung;[A12] however his experiments were performed for flow conditions that were much slower than those used in COCHISE, and the results cannot be extrapolated to COCHISE conditions reliably. Thus, the discharge experiments reported here provide an excellent demonstration of the feasibility of using an $Ar/N_2O$ discharge in the COCHISE experiments.

A12. Ung, A. Y.-M. (1975) A microwave discharge in $N_2O-N_2$ mixtures: A prolific source of oxygen atoms, Chem. Phys. Lett. 32:351.

47

Based upon the results of the flow reactor experiments, we estimate an $O/O_3$ ratio of $\sim 10^{-2}$ is attainable in the interaction volume. From Figure A1, if the reaction cell pressure can be maintained at $\sim 10$ mTorr by controlled heating of the cell walls, Reaction (A1) should form enough nascent $O_3(v)$ to detect by IR fluorescence.

The flow reactor results also provide information on possible deleterious effects due to the presence of N, NO, $O_2$, and unreacted $N_2O$ in the discharge effluent. It will be necessary to optimize the COCHISE discharges for these effects by observing NO, $N_2O$, and $O_3$ infrared emissions using an inert counter-flow gas.

Thus, we conclude that a nascent $O_3(v)$ observation in COCHISE using an $Ar/N_2O$ discharge mixture as a source of O is feasible if the apparatus can be operated successfully at elevated reaction cell pressures. The difficulties and uncertainties associated with elevated-pressure operation, together with the need to optimize the discharge conditions and gas mixtures, necessitate careful definition of these experiments before they commence. This effort is now in progress.

# References

A1.  Nadile, R.M., Stair, A.T., Jr., Wheeler, N.B., Frodsham, D.G.,
     Wyatt, C.L., Baker, D.J., and Griedler, W.F. (1978) SPIRE-Spectral
     Infrared Rocket Experiment (Preliminary Results), AFGL-TR-78-0107,
     AD A058504.

A2.  Green, B.D., Rawlins, W.T., and Caledonia, G.E. (1980) Interim Report
     on High Altitude Radiation Signatures, Physical Sciences Inc., TR-231.

A3.  Caledonia, G.E., Piper, L.G., Rawlins, W.T., and Green, B.D. (1980)
     Interim Technical Report: COCHISE Research, Physical Sciencies Inc.,
     TR-233.

A4.  Rawlins, W.T., Piper, L.G., Green, B.D., Wilemski, G., Goela, J.S.,
     and Caledonia, G.E. (1980) LABCEDE and COCHISE Analysis II,
     Vol. I, AFGL-TR-80-0063(1), AD A111837, Final Report, Contract
     AF19628-77-C-0089, Physical Sciences Inc., TR-207A.

A5.  Rawlins, W.T., Caledonia, G.E., and Kennealy, J.P. (1981) Observation of
     spectrally resolved infrared chemiluminescence from vibrationally
     excited $O_3(v_3)$, J. Geophys. Res. 86:5247.

A6.  Rawlins, W.T., and Armstrong, R.A. (1982) COCHISE Observations of $O_3$
     Formed by Three Body Recombination of O and $O_2$, AFGL-TR-82-0273,
     AD A123653.

A7.  West, G.A., Weston, R.E., Jr., and Flynn, G.W. (1976) Deactivation of
     vibrationally excited ozone by $O(^3P)$ atoms, Chem. Phys. Lett. 42:488.

A8.  Rosen, D.I., and Cool, T.A. (1973) Vibrational deactivation of $O_3(101)$
     molecules in gas mixtures, J. Chem. Phys. 59:6097.

A9.  Rosen, D.I., and Cool, T.A. (1975) Vibrational deactivation of $O_3$ molecules
     in gas mixtures. II. J. Chem. Phys. 62:466.

A10. Kennealy, J.P., DelGreco, F.P., Caledonia, G.E., and Green, B.D.
     (1978) Nitric Oxide chemi-excitation occurring in the reaction between
     metastable Nitrogen atoms and Oxygen molecules, J. Chem. Phys.
     69:1574.

A11.  Caledonia, G.E., Green, B.D., Simons, G.A., Kennealy, J.P., Robert, F.X., Corman, A., and DelGreco, F.P. (1977) COCHISE Studies I: Fluid Dynamical and Infrared Spectral Analyses, AFGL-TR-77-0281, AD A053218.

A12.  Ung, A.Y.-M. (1975) A microwave discharge in $N_2O-N_2$ Mixtures: A prolific source of oxygen atoms, Chem. Phys. Lett. 32:351.

# END

# FILMED

# 8-83

# DTIC